Cellular/Molecular

A New Vesicular Scaffolding Complex Mediates the G-Protein-Coupled 5-HT$_{1A}$ Receptor Targeting to Neuronal Dendrites

Sana Al Awabdh,[1,2] Stéphanie Miserey-Lenkei,[3] Tahar Bouceba,[4] Justine Masson,[1,2,5] Fumi Kano,[6] Carine Marinach-Patrice,[7] Michel Hamon,[1,2] Michel Boris Emerit,[1,2,5] and Michèle Darmon[1,2,5]

[1]INSERM U894, Centre de Psychiatrie et Neurosciences, Paris F-75014, France, [2]Université Pierre et Marie Curie—Paris 6, Faculté de Médecine Pierre et Marie Curie, Site Pitié-Salpêtrière, Paris F-75013, France, [3]Institut Curie, CNRS UMR144, Mécanismes Moléculaires du Transport Intracellulaire, Paris, France, [4]Institut de Biologie Intégrative, IFR83, Plateforme technique "Interactions Biomoléculaires en Temps Réel," Université Pierre et Marie Curie, Paris, France, [5]Université Paris Descartes, Sorbonne Paris Cité—Paris 5, UMR U894, Paris F-75014, France, [6]The University of Tokyo, Graduate School of Arts and Sciences, Tokyo 153-8902, Japan, and [7]INSERM UMR S945, Université Pierre et Marie Curie—Paris 6, Groupe Hospitalier Pitié-Salpêtrière, Service Parasitologie-Mycologie, Paris F-75013, France

Although essential for their neuronal function, the molecular mechanisms underlying the dendritic targeting of serotonin G-protein-coupled receptors are poorly understood. Here, we characterized a Yif1B-dependent vesicular scaffolding complex mediating the intracellular traffic of the rat 5-HT$_{1A}$ receptor (5-HT$_{1A}$R) toward dendrites. By combining directed mutagenesis, GST-pull down, and surface plasmon resonance, we identified a tribasic motif in the C-tail of the 5-HT$_{1A}$R on which Yif1B binds directly with high affinity ($K_D \approx 37$ nM). Moreover, we identified Yip1A, Rab6, and Kif5B as new partners of the 5-HT$_{1A}$R/Yif1B complex, and showed that their expression in neurons is also crucial for the dendritic targeting of the 5-HT$_{1A}$R. Live videomicroscopy revealed that 5-HT$_{1A}$R, Yif1B, Yip1A, and Rab6 traffic in vesicles exiting the soma toward the dendritic tree, and also exhibit bidirectional motions, sustaining their role in 5-HT$_{1A}$R dendritic targeting. Hence, we propose a new trafficking pathway model in which Yif1B is the scaffold protein recruiting the 5-HT$_{1A}$R in a complex including Yip1A and Rab6, with Kif5B and dynein as two opposite molecular motors coordinating the traffic of vesicles along dendritic microtubules. This targeting pathway opens new insights for G-protein-coupled receptors trafficking in neurons.

Introduction

Depression, one of the major public health issues in the world today, is mainly associated with deficits of serotonin (5-HT) neurotransmission (Stockmeier et al., 1998; Szewczyk et al., 2010). The most commonly prescribed class of antidepressants (selective serotonin reuptake inhibitors) inhibit the serotonin transporter to increase the level of extracellular serotonin, but 5-HT$_{1A}$ receptors (5-HT$_{1A}$Rs) initially counterbalance this action through their inhibitory control of serotonin release by raphe neurons. The therapeutic effect is reached only after 2–3 weeks of treatment corresponding to the slow desensitization of 5-HT$_{1A}$Rs (Le Poul et al., 1995). Thus, a way to accelerate the onset of antidepressant therapy could rely on acceleration of the slow desensitization of the 5-HT$_{1A}$R in raphe neurons (Bortolozzi et al., 2012). As the control of raphe neuron firing by 5-HT$_{1A}$Rs is linked to their dendritic localization (Riad et al., 2000), the identification of partner proteins implicated in their routing may unveil new targets for inhibiting 5-HT$_{1A}$R function in innovative therapies.

In our previous studies focused on the mechanism of the 5-HT$_{1A}$R targeting to dendrites, we have demonstrated that its C-terminus plays a key role in its dendritic localization and membrane targeting (Carrel et al., 2006), as it is also described for the targeting of other G-protein-coupled receptors (GPCRs) (Oksche et al., 1998; Duvernay et al., 2009). Whereas the trafficking of GPCRs presenting a PDZ interacting motif in their C-terminus tail has been extensively studied (Prybylowski et al., 2005; Bockaert et al., 2010), fewer data are available on the intracellular trafficking and sorting of serotonin receptors, which are devoid of this motif (Björk et al., 2010) as the 5-HT$_{1A}$R, a receptor exhibiting a very short C-tail.

We identified recently Yif1B, a membrane-bound protein whose interaction with the C-tail of the 5-HT$_{1A}$R is crucial for the distal dendritic targeting of this receptor in brain neurons. The specificity of this interaction is supported by the fact that Yif1B does not interact with the 5-HT$_{1B}$R, which is homologous to the

Received Dec. 20, 2011; revised July 17, 2012; accepted Aug. 8, 2012.

Author contributions: S.A., M.B.E., and M.D. designed research; S.A., S.M.-L., T.B., J.M., M.B.E., and M.D. performed research; F.K. contributed unpublished reagents/analytic tools; S.A., T.B., C.M.-P., M.H., M.B.E., and M.D. analyzed data; S.A., S.M.-L., M.H., and M.D. wrote the paper.

This research was supported by grants from INSERM and Université Pierre et Marie Curie. Confocal imaging was performed at the Plateforme Imagerie Cellulaire Pitié-Salpêtrière. S.A. was a recipient of fellowships from the French Ministère de la Recherche and the Fondation pour la Recherche Médicale during performance of this work. We are grateful to Cedric Pionneau (Plateforme P3S Post-Génomique, Pitié-Salpêtrière) for his contribution in Mass Spec analysis; Charbel Maroun for his expertise in the bioinformatic analyses of the protein sequences; Jean-Michel Camadro for his advices in BIAcore strategy; and Wanjin Hong for his generous gift of the GST-Yip1A plasmid.

The authors declare no financial conflicts of interest.

Correspondence should be addressed to Michèle Darmon, CPN, INSERM U894, 91 boulevard de l'Hôpital, 75634 Paris Cedex 13, France. E-mail: michele.darmon@inserm.fr.

DOI:10.1523/JNEUROSCI.6329-11.2012

 0270-6474/12/3214227-15$15.00/0

5-HT$_{1A}$R but restricted to the axonal compartment (Jolimay et al., 2000), and does not interfere either with the targeting of other types of somatodendritic receptors (Carrel et al., 2008).

In this study, we further characterized the molecular features of the direct interaction between the 5-HT$_{1A}$R and Yif1B, and we identified Yip1A, Rab6, and Kif5B as new intracellular partner proteins interacting with the 5-HT$_{1A}$R/Yif1B complex, which are crucial for the dendritic targeting of the receptor. On this basis, we propose a new vesicular trafficking pathway where Yif1B is a scaffold protein recruiting the 5-HT$_{1A}$R and these intracellular machinery proteins into vesicles, ensuring the transport along microtubules of the receptor toward distal dendrites.

Materials and Methods

Animals. Sprague Dawley rats (CERJ) were kept under controlled environmental conditions with free access to food and water until used for experiments. Experiments were performed in agreement with the institutional guidelines for the use of animals and their care, in compliance with national and international laws and policies (Council directives no. 87–848, October 19, 1987, Ministère de l'Agriculture et de la Forêt, Service Vétérinaire de la Santé et de la Protection Animale, permissions no. 75–974 to M.D. and no. 75–976 to M.B.E.).

Antibodies. The following primary antibodies were used: rabbit anti-green fluorescent protein (GFP) antibody (Millipore Bioscience Research Reagents; 1:1000), mouse monoclonal anti-α-tubulin antibody (Abcam, 1:2000), rabbit anti-tubulin antibody (Novus Biologicals, 1:1000), rabbit anti-MAP2 antibody (Millipore Bioscience Research Reagents, 1:1000), mouse monoclonal anti-Flag M2 antibody (Sigma; 1:2000), rabbit polyclonal anti-uKHC (Kif5B) antibody (H-50, Santa Cruz Biotechnology, 1:1000), mouse monoclonal anti-dynein (intermediate chain) antibody (Sigma-Aldrich, 1:1000), mouse anti-P150Glued (BD Transduction Laboratories 1:500). Rabbit anti-Yif1B antibody was purified as described previously (Doucet et al., 2007; Carrel et al., 2008) and used at 1:1000. Rabbit anti-Rab6 antibody (C-19, Santa Cruz Biotechnology, 1:100) and rabbit anti-Yip1A antibody (1:100) were described previously (Kano et al., 2009). The secondary antibodies used were Alexa Fluor 405-, 488-, and 568-conjugated antibodies from Invitrogen (1:500, 1:2000, and 1:1000, respectively), and HRP-conjugated anti-rabbit and anti-mouse antibodies (Sigma; 1:10,000).

Plasmid constructs and site-directed mutagenesis. The plasmids encoding rat 5-HT$_{1A}$R-eGFP (Carrel et al., 2008) and sst2A-eGFP (Lelouvier et al., 2008) have already been used and described. The C-terminal fluorescent-tagged proteins were cloned using the Infusion PCR Cloning System (Clontech) into the HindIII site of pEYFP-N1 vector, pCherry-N1 vector, or peGFP-N1 vector (Clontech).

The primers used were respectively: forward primer 5′-TCTCGAGC TCAAGCTTCATGGATGTGTTCAGTTTTGGC-3′, and reverse primer 5′-GCAGAATTCGAAGCTTTGATCGGCGGCAGAACTTGCA-3′ for the rat 5-HT$_{1A}$R sequence (Albert et al., 1990); forward primer 5′-TCTC GAGCTCAAGCTTATGCACGCGACAGGTTTG-3′ and reverse primer 5′-GCAGAATTCGAAGCTTTGACCGTACAAGGTGGAAGGT-3′ for the rat Yif1B sequence. The rat Yip1A sequence (NM_001014150.3) was amplified on cDNA reverse transcribed from rat brain mRNA with the forward primer ATGTCAGGCTTTGATAACTTAAACAGCGG (nucleotides 104–132 NM_001014150.3) and reverse primer TCAAAAGACG GAAATCAGGGCAAAG (nucleotides 853–877 NM_001014150.3), and cloned into TA cloning vector (Invitrogen). The Yip1Acherry plasmid was constructed after amplification with the forward primer CCCAAG CTTCCACCATGTTCAGGCTTTGATAACTTAAAC and the reverse primer CGGGGTACCGTAAAGACGGAAATCAGGGCAAAG, digested with HindIII and KpnI, and ligated with the HindIII KpnI linearized pCherryN1 vector. The N-terminal truncated Yif1B proteins tagged with a Flag epitope were generated by amplification with the following primers (the HindIII site is in italics) and inserted at the *Hind*III site of the pFlag-CMV-6a vector (Sigma): Yif1B fw HindIII: 5′-GCGAAGCTTTTATGCACGCGAC AGGTTTG-3′; Flag-Yif1B(10) fw HindIII: 5′-GCGAAGCTTTTGGGACGC CCCGGCTGCGTAAG-3′; Flag-Yif1B(18) fw HindIII: 5′-GCGAAGCTTT TCCCTCAAAGCGGAGGGTCCC-3′; Flag-Yif1B(30) fw HindIII: 5′-GCGAAGCTTTTATGGCTGATCCCCACCAGTTT-3′; Flag-Yif1B(50) fw HindIII: 5′-GCGAAGCTTTTGGCCAGCCATCACCTGGTAGC-3′; and Flag-Yif1B(55) fw HindIII:5′-GCGAAGCTTTTATGGGTAGCCTGGGT TACCCCACC-3′.

The C-terminal truncated Yif1B proteins were generated after amplification with the following oligos, the reverse primer containing a stop codon (in italics), and inserted between the HindIII and the EcoRI sites of the pCB6 vector (Brewer and Roth, 1991) downstream of the CMV promoter: Yif1B 1 fw HindIII: 5′-GCGAAGCTTTTATGCACGCGACAGGT TTG; Yif1B 311 rev EcoR1: 5′-AGAATTC*TCA*CCGTACAAGGTGGAAG GT-3′; Yif1B(152) rev EcoR1: 5′-AGAATTC*TCA*TGGAGCATTGATGT CAAAGCG-3′; Yif1B(186) rev EcoR1: 5′-AGAATTC*TCA*CTGTAGTC CCAGGAGGTCTGG-3′; Yif1B(220) rev EcoR1: 5′-AGAATTC*TCA* CACCAGGTCAATGGTGGTAA-3′; and Yif1B(272) rev EcoR1: 5′-AGAATTC*TCA*TGCCTGGGCCAGGATCTTGAG-3′.

The His-Yif1BNt plasmid corresponding to the N-terminal cytoplasmic domain (amino acids 1–152) of the rat Yif1B was generated after amplification with forward primer 5′-TGGGAATTCGAAGCTT TATGCACGCGACAGGTTTGGCG-3′ and reverse primer 5′-CAAA ACAGCCAAGCTTTCATGGAGCATTGATGTCAAAGCG-3′, and cloned in the HindIII site of the pTrcHis-A vector (Invitrogen) using the Infusion PCR Cloning System (Clontech) for N-termini His-tagged fusion protein production.

The QuikChange Site-Directed Mutagenesis Kit (Stratagene) was used to generate mutants within the C-terminal cytoplasmic domain (amino acids 406–422) of the rat 5-HT$_{1A}$R (Albert et al., 1990) cloned in pGEX-6p1 for GST-tagged fusion protein production (GST-CT1A), or within the rat Flag-5-HT$_{1A}$R, the Flag-YifB, or the His-Yif1BNt (Carrel et al., 2008). Only the sense oligonucleotides are listed below, with the mutated nucleotides in bold letters: GST-CT1A: K405A: GGCCGCACTAGCC**GC**AGACTTTCAAAAC GC; *K412A*: CAAAACGCTTTT**GC**GAAGATAATCAAGTGC; R421A: GT GCAAGTTCTGC**GC**CCGATGAGGATCC; R422A: GTGCAAGTTCTG CCGC**GC**ATGAGGATCC; R421/422A: GTGCAAGTTCTGC**GC**C**GC**AT GAGGATCC; C417/420S: AAGATAATCAAG**A**GCAAGTTC**A**GCCGCC GATGAGAATTC; I414/415A: CGCTTTTAAGAAG**GC**A**GC**CAAGTGCA AGTTCTGCCG; Q408: GCCAAAGACTTT**GC**AAACGCTTTTAAG; Flag-5-HT$_{1A}$R: Flag K405A: TATGCTTATTTCAAC**GC**AGACTTTCAAAAC GCT; Flag R421/422: GTGCAAGTTCTGC**GC**C**GC**ATGAGGATCC; His-Yif1BNt: D33A: GGGCATGGCTG**C**TCCCCACCAGTTT; D39/40AA: CTGATCCCCACCAGTTTTTTG**C**CG**C**CACGAGTTCA.

For the multiple substitutions, successive reactions were performed. All constructions were confirmed by sequencing the entire insert.

RNA interference. For silencing Rab6, Yip1A, and Kif5B expression, we used siRNAs (Sigma, Invitrogen and ThermoScientific) directed against human and rat: Rab6A/A′ (GACAUCUUUGAUCACCAGA) (*CAC-CUAUCAGGCAACAAUU*) (Del Nery et al., 2006); Rat Yip1A (GGAUAUCUGUGGGCCGGAUUCAU); Rat Kif5B (GCACAUCU-CAAGAGCAAGUUU); and control siRNA (CCAGUACUUCGUA-CUCCAAUCGACA) (Carrel et al., 2008). siRNAs were transfected into hippocampal neurons with Lipofectamine 2000 or RNAiMax (Invitrogen) (160 nM final concentration).

Cell culture and transfection. Neuronal cultures were made as described previously (Goslin et al., 1998; Carrel et al., 2008) with some modifications. Hippocampi of rat embryos were dissected at day 17–18. After trypsinization, tissue dissociation was achieved with a Pasteur pipette. Cells were counted and plated on poly-D-lysine-coated 15-mm-diameter coverslips, at a density of 300–375 cells/mm^2, in complete Neurobasal medium supplemented with B27 (Invitrogen), containing 0.5 mM L-glutamine, 10 U/ml penicillin G, and 10 mg/ml streptomycin. Three hours after plating, the medium was replaced by a conditioned medium obtained by incubating glial cultures (70–80% confluency) for 24 h in the complete medium described above. Hippocampal neurons were transfected on the day *in vitro* 7 (DIV7) to DIV8 as follows: for each coverslip, plasmid DNA (2.5 μg) was mixed with 50 μl of Neurobasal medium without B27 supplement. After 15 min at room temperature, 1.25 μl of Lipofectamine 2000 in 50 μl of Neurobasal medium was added, and incubation continued for another 30 min. After the addition of 150 μl of complete Neurobasal medium containing B27 supplement, the mix was applied to the neuronal culture, and transfection lasted for 3 h at

37°C. Typically, 5–10% of neurons expressed the receptors after transfection. For cotransfection experiments in the presence of siRNA, the plasmids (2 μg) and the siRNA (2 μl of a 20 μM solution) were separately mixed either with Lipofectamine 2000 (0.5 μl/coverslip) or RNAimax (0.5 μl/coverslip) and mixed before addition to neurons. COS-7 cells were grown in DMEM GlutaMAX™I (Invitrogen) supplemented with 1 g/L glucose, 10% fetal bovine serum, 10 U/ml penicillin G, and 10 g/ml streptomycin. COS-7 cells (50% confluent) were transfected using FuGENE (Roche) according to the manufacturer's protocol. HeLa cells and LLCPK1 cells expressing stably Yif1B were grown in DMEM GlutaMAX™I (Invitrogen) supplemented with 4.5 g/L glucose, 10% fetal bovine serum, 10 U/ml penicillin G, and 10 g/ml streptomycin; 0.7 μg/μl geneticin (G418) was added for the stably expressing cells. HeLa cells (80% confluent) were transfected using Lipofectamine 2000 reagent (Invitrogen) according to the manufacturer's protocol. For both cell lines and hippocampal neurons, receptor expression was allowed in growth medium for 48 h after transfection. Protein expression for GST pull-down experiments was allowed in growth medium for 24 h after transfection.

Indirect immunofluorescence. Cells on coverslips were washed with D-PBS+ (D-PBS containing 0.1 mM $CaCl_2$ and 0.1 mM $MgCl_2$) at 37°C, then fixed with paraformaldehyde (3%) containing 4% sucrose at 37°C in D-PBS− and permeabilized with 0.1% Triton X-100 in D-PBS−. After 2× 10 min washes in D-PBS+, cells were incubated for 30 min in antibody buffer (3% bovine serum albumin, 2% normal goat serum, and 2% normal donkey serum in D-PBS−). Incubation with primary antibodies was then performed in antibody buffer for 1 h at room temperature. After 2× 10 min washes in D-PBS−, incubation with secondary antibodies proceeded for 1 h. The secondary antibodies used were Alexa Fluor-conjugated donkey anti-rabbit or anti-mouse IgG. The coverslips were finally mounted in Fluoromount-G solution (Clinisciences). Immunofluorescence images were generated using a Leica TCS SP2 AOBS laser scanning confocal microscope (40, 63, or 100 × oil-immersion lens). Background was lowered using Gaussian blur (radius 1 pixel), and the contrast and brightness of images displayed in figures were modified using Adobe Photoshop CS2 for clearer demonstration and do not correspond to the analysis conditions.

Quantification of dendrite fluorescence. The contrast and brightness of confocal images were chosen to ensure that all relevant pixels were within linear range and were maintained to be identical for all measurements. For double-labeling experiments, pictures were generated using Adobe Photoshop CS2. Fluorescence profiles along dendrites were generated using the Lucia 4.71 software (Nikon). For the comparison of 5-HT$_{1A}$R-eGFP receptor distribution, all neurons showing intact morphology along their longest dendrite, with unambiguous visual identification of the axon, were analyzed (one dendrite per neuron). The variability of distribution in individual neurons was eliminated by using the cumulated fluorescence profiles obtained for 20 neurons in each group (see Figs. 2, 8). Mean fluorescence between 50 and 100 μm was calculated for 20 neurons for each condition and then normalized to the mean value of the control condition. Data analysis was performed with GraphPad software. All results are reported as the mean ± SEM. Statistical significance was assessed by using Student's *t* test or one-way ANOVA with Bonferroni's or Dunnett's *post hoc* tests. The level of significance was set at $p < 0.05$.

Time-lapse fluorescence videomicroscopy. Experiments were performed on transfected hippocampal neurons grown on 35 mm glass base dishes (IWAKI) with culture medium supplemented with 20 mM HEPES. Time-lapse imaging was performed 48 h after transfection at 37°C using a spinning-disk microscope mounted on an inverted motorized confocal microscope (Leica TCS SP2) through a 100× 1.4 numerical aperture PL-APO objective lens. The apparatus was composed of a Yokogawa CSU-22 spinning disk head, a Roper Scientific laser lounge, a Photometrics Coolsnap HQ2 CCD camera for image acquisition, and MetaMorph software (MDS) to control the setup. Acquisition parameters were 50–200 ms exposure for the GFP and Cherry channels. The laser was set to 30% in each case. Movies in supplemental material provided correspond to stacks resulting from a maximal intensity projection through the *z*-axis performed with the MetaMorph software (NIH Image). Trajectories of moving vesicles were tracked with the MTrackJ Plugin of ImageJ software developed by Erik Meijering at the Biomedical Imaging Group Rotterdam of the Erasmus MC-University Medical Center Rotterdam (The Netherlands). Trajectories were classified as anterograde or retrograde according to their direction in dendrites or as somatic if the traffic occurred only in the soma. Mean and SEM values were calculated and plotted using GraphPad 4 Software. Statistical significance was assessed by using one-way ANOVA with Bonferroni's *post hoc* test.

GST pull-down assay. GST-tagged fusion proteins were produced in the BL21DE3 strain of *Escherichia coli* (Stratagene). After induction for 3 h with 0.5 mM isopropyl-β-D-thiogalactopyranoside at 28°C for the GST-CT1A and GST-Yip1A, and at 37°C for the GST-Rab6, the bacterial pellet was sonicated in PBS (10 ml/250 ml of culture), 0.1% Triton X-100, and protease inhibitors (Sigma), and centrifuged at 14,000 × *g* for 15 min. Supernatants were incubated overnight with glutathione-Sepharose beads (GE Healthcare) at 4°C, then washed in PBS. Extracts from Yif1B transfected stable LLC-PK1, COS7, or HeLa cells expressing the different forms of truncated Yif1B or from hippocampus, raphe, and cerebellum dissected from Sprague Dawley male rats were homogenized by sonication in buffer A (20 mM HEPES, pH 7.4, 150 mM NaCl, 2 mM EDTA, 0.5% NP-40, protease inhibitors, 1 ml/100 mg of tissue). After centrifugation at 15,000 × *g* for 10 min, 100–200 μg of proteins from cell lysates or 1 mg of proteins from tissue homogenates were incubated with glutathione-Sepharose beads coupled to the different GST fusion proteins in buffer B (buffer A containing 2.5 mg/ml bovine serum albumin), overnight at 4°C. After washing twice with buffer B, and then one time with buffer A, the proteins retained on the beads were eluted in sample buffer (Laemmli, 1970) and loaded by SDS-PAGE gel, followed by blotting to PVDF membrane and incubation with Yif1B affinity-purified antiserum (1:2000). For surface plasmon resonance (SPR) analysis the proteins retained on the beads were eluted with buffer C [10 mM glutathione reduced form (Sigma), 50 mM Tris-HCl, pH 8) and dialyzed in HBS-EP buffer (10 mM HEPES, 150 mM NaCl, 3 mM EDTA, 0.005% Tween-20). For proteomic analysis, the beads were washed two times with buffer B and three times with buffer A, then incubated overnight with 10 units of PreScision Protease (GE Healthcare) at 4°C. After centrifugation at 106 × *g* for 5 min, the supernatant was cleared with Glutathione-Sepharose beads (GE Healthcare) at 4°C for 7 h.

Purification of recombinant His-Yif1B. The His-tagged fusion protein was produced in the BL21DE3 strain of *E. coli* (Stratagene). After induction at 37°C for 3 h with 1 mM isopropyl-β-D-thiogalactopyranoside, the bacterial pellet (10 ml/250 ml of culture) was homogenized and incubated for 30 min at 4°C in buffer BW [20 mM NaH_2PO_4, 50 mM NaCl, 40 mM imidazole, 1 mg/ml lysozyme (Eurobio), and protease inhibitors (Sigma)], sonicated, and centrifuged at 14,000 × *g* for 30 min. Supernatants were incubated for 3 h with Nickel-Sepharose beads (GE Healthcare) at room temperature. After washing five times in buffer BW, the proteins retained on the beads were eluted in buffer EB (20 mM NaH_2PO_4, 50 mM NaCl, 500 mM imidazole, 50 mM EDTA, and protease inhibitors). The eluates were dialyzed in HBS-EP buffer for SPR analysis.

Surface SPR. Binding experiments and kinetic assays were performed at 25°C using Biacore 3000 SPR sensor with control software version 4.1 and Sensor Chip CM5 (carboxymethylated dextran surface). Proteins were immobilized via amine groups. To this end, the chip surface was first activated according to the recommendations of the Biacore amine coupling kit by injecting 70 μl of a mixture (1:1, v/v) of 100 mM NHS (N-hydroxysuccinimide) and 400 mM EDC (1-ethyl-3-(3-dimethyl-aminopropyl) carbodiimide). Purified His-Yif1B proteins (mutated or not, 100 μg/ml in 10 mM sodium acetate, pH 4) were then injected (flow rate: 10 μl/min, for its immobilization) followed by a 7 min injection of 1 M ethanolamine, pH 8.5, to inactivate the residual active groups. Binding and kinetic analysis were performed by injecting the purified GST-CT1A proteins (mutated or not) at a flow rate of 5 μl/min for 5 min using HBS-EP as the running buffer, dissociation was observed for 10 min before the elution of the analyte. Regeneration was then performed by injection of 10 mM glycine-HCl, pH 2.0, at a flow rate of 30 μl/min with a contact time of 30 s. GST alone was injected as a negative control in the same condition. Data were analyzed with BIA evaluation 4.1 software (Biacore).

Proteomic analysis. The supernatants obtained after GST pull down were eluted in sample buffer (Laemmli, 1970) and separated in a one-dimensional 12% SDS-PAGE gel, followed by Colloidal Blue staining (Invitrogen). Gel lanes were washed twice with 25 mM ammonium bicarbonate in 50% acetonitrile then dehydrated in 100% acetonitrile, before being subjected to overnight in-gel trypsin digestion. Briefly, each spot was digested with a solution containing 50 mM ammonium bicarbonate, 10% acetonitrile, and 20 ng/μl trypsin (G-Biosciences) on ice over 1 h, then overnight at 37°C. The supernatants were collected and gel plugs were incubated in 0.1% trifluoroacetic acid (TFA), 50% acetonitrile in an ultrasonic bath over 10 min to extract residual peptides. The new supernatants were pooled to the former. Peptides were dried completely in a vacuum centrifuge then resuspended in 0.1% TFA, 50% acetonitrile, to be analyzed by mass spectrometry (MS/MS) (Shevchenko et al., 2006; Perrot et al., 2011). MS/MS analysis was performed using the Ultimate 3000 nano LC system (Dionex) coupled to an Esquire HCTultra nESI-IT-MS (Bruker Daltonics). Gradient used and mass spectrometer parameters were as described previously (Escoffier et al., 2010). Liquid chromatography-MS/MS experiments were processed with Data Analysis software (Bruker Daltonics) to create a single MASCOT generic file (MGF). MGF files were used to search in the NCBI human protein database [ftp://ftp/ncbi.nlm.nih.gov/ (downloaded in December 2007)] using MASCOT (Mascot Daemon, version 2.2, Matrix Science). The search parameters were as follows: 1+, 2+, and 3+ charged peptides, one missed cleavage, mass tolerance of 0.5 Da for peptides, and MS/MS, carbamidomethyl and methionine oxidation were permitted. Confident matches were defined by the MASCOT score and statistical significance ($p < 0.05$), the number of matching peptides, and the percentage of the total amino acid sequence covered by matching peptides.

Results

A tribasic motif in the C-tail of the 5-HT$_{1A}$R interacts directly with a triacidic motif in the N-tail of Yif1B

We have previously shown (Carrel et al., 2008) that Yif1B interacts with the C-tail of the 5-HT$_{1A}$R to specify its dendritic localization. To determine which domain of Yif1B interacts with 5-HT$_{1A}$R, we performed GST pull-down experiments with several truncated forms of Yif1B (Fig. 1*A*). The 5-HT$_{1A}$R C-tail tagged with GST (GST-CT1A) was used as a bait to pull down Yif1B truncated forms from transfected cell extracts (Fig. 1*B*). The C-tail of Yif1B was not involved in the interaction with 5-HT$_{1A}$R since Yif1B proteins truncated in their C-terminal part (1–152, 1–186, 1–220) still interacted with GST-CT1A but not with GST alone (Fig. 1*A*,*B*). Despite its low expression, the N-tail of Yif1B (1–152) was found to be sufficient to interact with GST-CT1A (Fig. 1*B*), thereby assigning the interaction domain to this segment. GST pull-down experiments with the different N-terminal truncated forms (10–311, 18–311, 30–311, 50–311, 55–311; Fig. 1*A*) indicated that the interaction was lost when the first 50 aa were deleted (Fig. 1*C*). The loss of affinity of Yif1B truncated forms was probably not attributable to a general change of conformation since no secondary structure could be predicted in the first 70 aa of Yif1B, probably due to the presence of 10 proline residues among a total of 18 proline residues found in Yif1B (data not shown). To characterize the interaction between the 5-HT$_{1A}$R and Yif1B, and to determine its affinity, we used SPR and Biacore analysis. Because purified hydrophilic proteins were required, we chose to immobilize on the sensor chip the N-tail of Yif1B (ligand) tagged with a His-tag on its N-terminal end (His-Yif1B-NT) sufficient for the interaction with the receptor. GST-CT1A was loaded in fluid phase (analyte) over the sensor chip, and GST alone was used as a negative control. Binding analysis showed that the C-tail of the 5-HT$_{1A}$R interacted directly with Yif1B, whereas no binding was detected with GST alone (Fig. 1*D*,*F*). Kinetic analyses with various concentrations of GST-CT1A (Fig. 1*D*) allowed estimation of association and dissociation rates corresponding to a K_D value of 37 nM, indicating a high affinity between the 5-HT$_{1A}$R and its partner Yif1B. To identify the motifs in the C-tail of the 5-HT$_{1A}$R that were involved in the interaction with Yif1B, we performed site-directed mutagenesis. Previous data showed that Yif1B interacts with the 5-HT$_{1A}$R, but not with the 5-HT$_{1B}$R (Carrel et al., 2008), despite a strong homology between the respective sequences of their C-tails. Accordingly, we mutated amino acid residues that were specific of the 5-HT$_{1A}$R with regard to the 5-HT$_{1B}$R (e.g., I414, I415, Q408, C417, C420, R421, R422, K405, F412). GST pull-down experiments were performed with the mutated GST-CT1A (Table 1) as baits on rat brain extracts expressing endogenous Yif1B. With this technique, most of the mutants were able to interact with Yif1B and only two mutated forms of the fusion proteins: the K405/R421/R422A (also called KdiR) and K405/K412/R421/R422A (also called diKdiR) totally lost this capacity (Fig. 1*E*,*F*). Binding affinities between His-Yif1B-NT (grafted on a chip) and the same GST-CT1A mutants were estimated by SPR (Table 1). Mutations of the motifs identified previously in the C-tail (Carrel et al., 2006) that interfered with the proper surface expression of the 5-HT$_{1A}$R (i.e., the di-isoleucine motif I414/415A with or without the additional mutation of the Q408, or mutations of the terminal cysteines C417/420S) did not decrease the affinity for Yif1B (Table 1). However, the mutations R421A, R422A, and K405A yielded a moderate shift of affinity, while the double mutation R421/422A resulted in a 100-fold decrease in affinity. An additional mutation of the third basic residue K405 in the R421/422A (KdiR) completely abolished the interaction with Yif1B. As the mutant K412diR still exhibited an affinity similar to that of the double mutant R421/422A, in contrast to K405diR, which no longer interacted with Yif1B, we can suppose that the position of the third basic residue is important (Table 1). We concluded that the C-tail of the 5-HT$_{1A}$R contains a tribasic motif crucial for the interaction with Yif1B. This motif is composed of the lysine 405 and the two arginines in position 421–422. Interestingly, we observed that the mutant 5-HT$_{1A}$R with the KdiR mutation (Fig. 2*B*), which did not interact with Yif1B, remained confined in the soma and proximal dendrites, and was less targeted to distal dendrites than the WT 5-HT$_{1A}$R (Fig. 2*A*), supporting the idea that the interaction with Yif1B plays a key role in the targeting of the 5-HT$_{1A}$R. The profile of the cumulated fluorescent intensity along the longest dendrite shows a difference between the WT and mutated 5-HT$_{1A}$R (Fig. 2*C*). The mean fluorescence calculated for the 50–100 μm distance from the soma was significantly different (unpaired *t* test, $F_{(1,46)} = 3.217$, $p = 0.0024$) between WT [mean fluorescence intensity (F.I.) = 149.7 ± 11.8, $n = 24$] and mutated 5-HT$_{1A}$R (mean F.I. = 11.8 ± 8.8, $n = 24$). Accordingly, the KdiR mutant was used in most of the subsequent experiments as a negative control that does not interact with Yif1B and is not targeted to distal dendrites.

We then investigated which motif in the N-terminal tail of Yif1B was important for its interaction with the 5-HT$_{1A}$R. Interestingly, only three acidic residues are found among the first 50 aa of its sequence. To assess whether these amino acids could form the interacting motif facing the three basic residues of the 5-HT$_{1A}$R C-tail, we first performed GST pull-down experiments using WT and KdiR GST-CT1A as baits with cell extracts expressing Flag-Yif1B: WT, 1DA (D33A), 2DA (D39/40AA), and 3DA (D33/39/40AAA; Table 1, sequence). Whereas no decrease of binding was observed when the two aspartates were mutated, the 3DA Flag-Yif1B was scarcely pulled down (Fig. 1*G*). This result

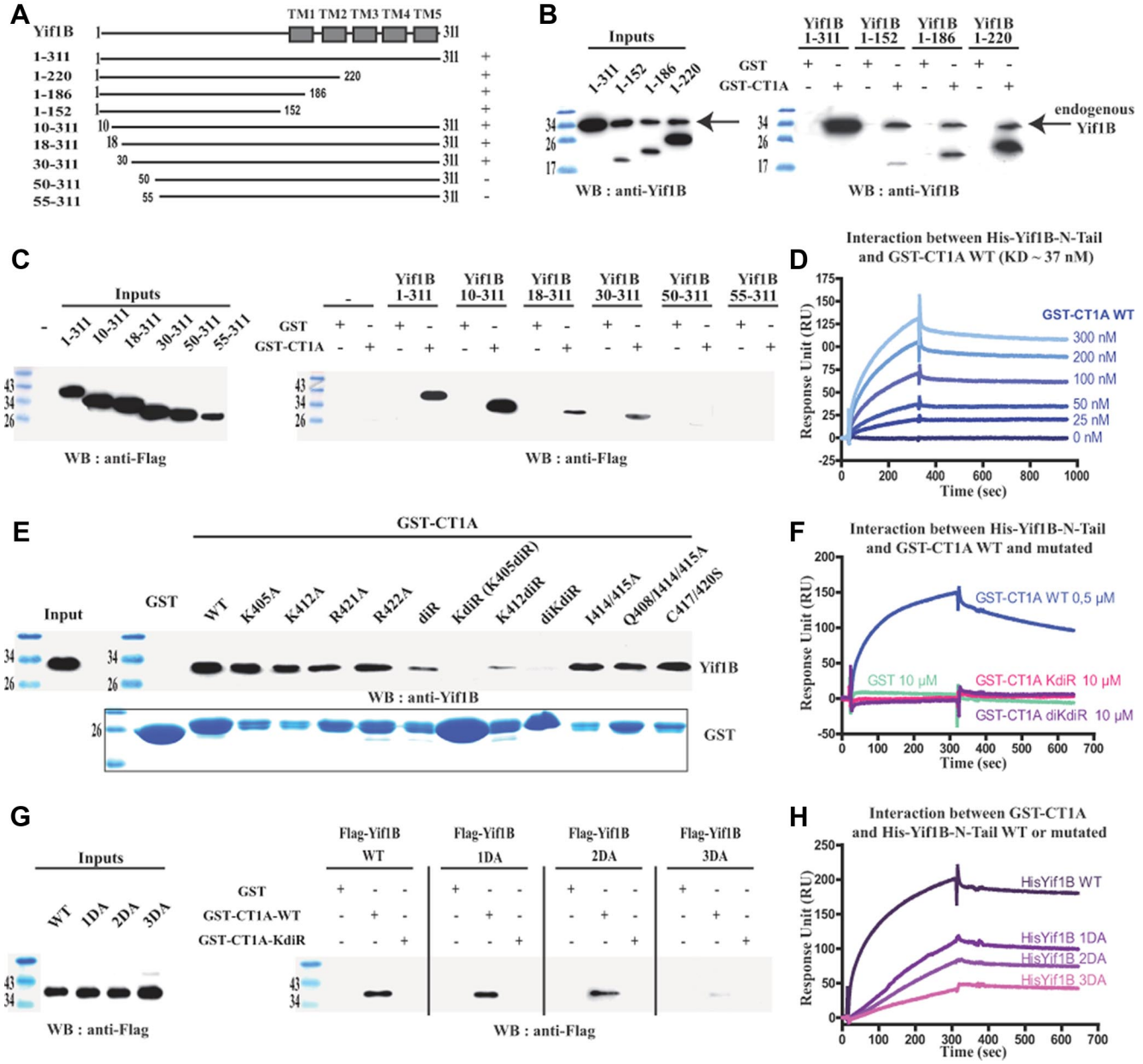

Figure 1. Characteristics of the 5-HT$_{1A}$R/Yif1B interaction. ***A***, Schematic representation of the different Yif1B constructs used in this study. Boxes represent the transmembrane domains (TMs). Interaction with the C-tail of the 5-HT$_{1A}$R is indicated (±). ***B***, ***C***, Purified WT GST-CT1A or GST alone (control) was incubated with HEK cell lysates expressing the different truncated Yif1B forms (Inputs, left panels). ***D***, Surface plasmon resonance (SPR) determination of the association and dissociation constants for the interaction between WT GST-CT1A and WT His-Yif1B. The concentration range of GST-CT1A was 0–300 nM in six serial concentrations passed on His-Yif1B immobilized on a sensor chip ($n = 3$). Data are presented as real-time graphs of response unit (RU) against time and were analyzed using a 1:1 Langmuir binding model to determine the K_D value reported in Table 1. ***E***, ***G***, Purified GST-CT1A (WT, KdiR, and other mutants) and GST alone (negative control) were incubated with rat brain lysates (***E***), or HeLa cell lysates expressing the different Flag-tagged mutated Yif1B (***G***). GST proteins were visualized using Coomassie Blue (***E***, bottom). Inputs represent a 2.5% load of the total lysates used in all conditions. GST pull-downs were analyzed by Western blot followed by ECL+ detection (right panels) using anti-Yif1B antibody (***B***, ***E***) or anti-Flag antibody (***C***, ***G***). ***F***, ***H***, SPR analyses of the binding of various mutated and WT forms of His-Yif1B with WT or mutated GST-CT1A. WT His-Yif1B (***F***) and mutated His-Yif1B (***H***) were each immobilized on a sensor chip. Binding assays with 500 nM WT GST-CT1A, 10 µM mutated GST-CT1A mutants KdiR or diKdiR (***F***), and 10 µM GST alone (***F***, ***H***) used as a negative control were passed over the chip ($n = 3$). Data are presented as real-time graphs of RU against time.

was supported by SPR binding experiments with mutated His-Yif1B N-tail (1DA, 2DA, and 3DA): we observed a reduction of the resonance unit intensity that increased with the number of mutated acidic residues (Fig. 1*H*). Furthermore, mutation of the third aspartate residue increased by 10-fold the K_D of the interaction in comparison with the 2DA mutant (Table 1). We concluded that the 5-HT$_{1A}$R/Yif1B interaction involves at least three basic amino acid residues of the C-tail of the 5-HT$_{1A}$R that are facing three aspartic acid residues located between the 30th and 50th amino acids in the N-tail of Yif1B.

Yif1B is the scaffold protein between the 5-HT$_{1A}$R, Yip1A, and Rab6

Because it is unlikely that such a ubiquitous protein as Yif1B can alone play a specific role in the dendritic targeting of the 5-HT$_{1A}$R, we searched for other proteins implicated in the trafficking of the receptor. Proteins interacting with the C-tail of the 5-HT$_{1A}$R (GST-CT1A) were pulled down from rat brain lysates and sequenced by mass spectrometry. Among the bound proteins (Fig. 3*A*), we identified Rab6 and tubulin (α2 and β2 isoforms). Rab6 is a Golgi-associated protein implicated in anterograde

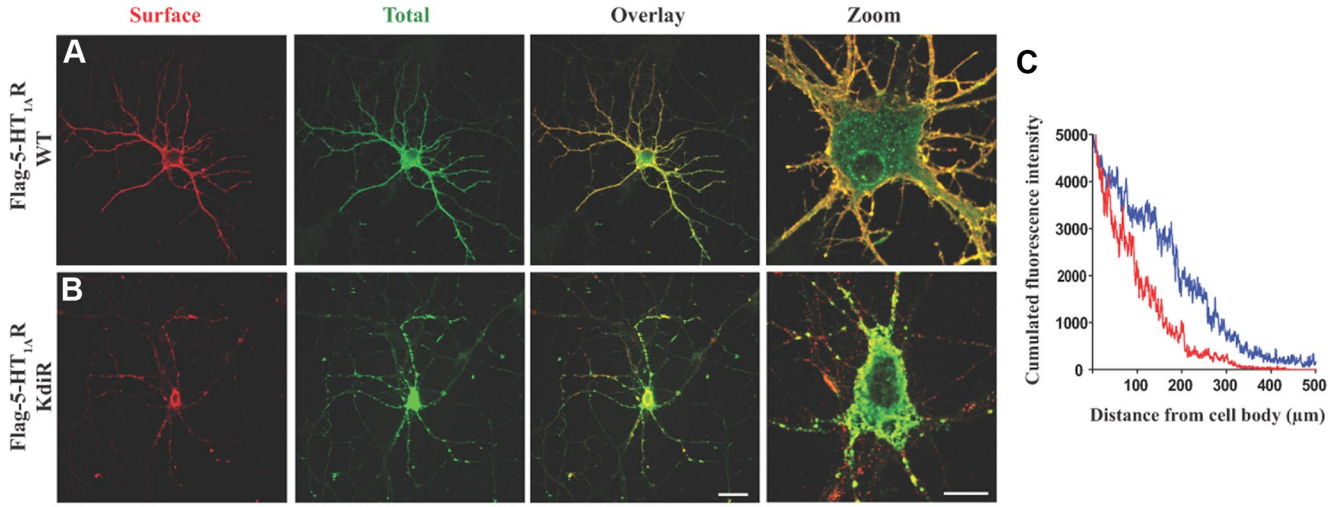

Figure 2. The KdiR mutation disturbs the targeting of the 5-HT$_{1A}$R. ***A***, ***B***, Expression of the Flag-5-HT$_{1A}$R WT (***A***) and the Flag-5-HT$_{1A}$ KdiR mutant (***B***) 48 h after transfection of hippocampal neurons. Comparison of surface staining with mouse monoclonal anti-Flag antibody (red) and total labeling with the rabbit anti-Flag (green) after plasma membrane permeabilization. Scale bars: (in ***B***) Overlay, 50 μm; Zoom, 10 μm. ***C***, The profile of the cumulated fluorescence intensity of the receptor (cumulated F.I., arbitrary unit) along the longest dendrite (μm), in blue for the Flag-5-HT$_{1A}$R WT, and in red for the KdiR mutant (surface, total, overlay). The mean cumulated fluorescence intensity along the 50–100 μm length from the soma shows a significant difference between the WT (mean F.I = 149.7 ± 11.8, $n = 24$) and the mutated 5-HT$_{1A}$R (mean F.I. = 11.8 ± 8.8, $n = 24$) (unpaired t test, $F_{(1,46)} = 3.217$, $p = 0.0024$).

Table 1. Analyses of the surface plasmon resonance (SPR) kinetic data of the binding of 5-HT$_{1A}$R (WT vs mutants) with Yif1B (WT vs mutants)

Protein names	Mutation positions	K_D (nM)	χ^2
GST-CT1A WT or mutants			
GST-CT1A WT	405**K**DF**Q**NAF**KK**I**I**K**C**KF**CRR**422	37	0.722
I414/415A	KDFQNAFKK**AA**KCKFCRR	44	1.43
Q408/I414/415A	KDF**A**NAFKK**AA**KCKFCRR	21	1.63
C417/420S	KDFQNAFKKIIK**S**KF**S**RR	14	7.38
R421A	KDFQNAFKKIIKCKFC**A**R	77	0.187
R422A	KDFQNAFKKIIKCKFCR**A**	110	1.52
R421/422A	KDFQNAFKKIIKCKFC**AA**	2900	0.967
K405A	**A**DFQNAFKKIIKCKFCRR	200	1.81
K412A	KDFQNAF**A**KIIKCKFCRR	71	0.184
K405/R421/422A or KdiR	**A**DFQNAFKKIIKCKFC**AA**	ND	ND
K412/R421/422A or K412diR	KDFQNAF**A**KIIKCKFC**AA**	5600	0.304
K405/K412/R421/422A or diKdiR	**A**DFQNAF**A**KIIKCKFC**AA**	ND	ND
Yif1B-N-Tail WT or mutants			
Yif1B WT	28QPGMA**D**PHQFF**DD**TSSAP44	37	0.722
1DA	QPGMA**A**PHQFFDDTSSAP	27	1.73
2DA	QPGMADPHQFF**AA**TSSAP	20	1.13
3DA	QPGMA**A**PHQFF**AA**TSSAP	193	0.495

Estimates of the association and dissociation constants were obtained from kinetic analyses performed with the N-tail of His-Yif1B (WT or mutants) immobilized on the sensor chips and six serial concentrations of GST-CT1A (WT or mutants) passed on the chip in fluid phase. Mutated residues are in bold type in the amino acid sequences. K_D values were calculated using BiaEval software by fitting the Biacore sensorgram with the 1:1 Langmuir model, χ^2 test < 10. The KdiR and the diKdiR GST-CT1A mutants did not bind to Yif1B. Therefore, it was not possible to calculate affinity constants. ND, Not determined.

(Grigoriev et al., 2007) and retrograde traffic (White et al., 1999; Del Nery et al., 2006) of vesicles from the Golgi that has also been shown to participate in the membrane targeting of some GPCRs (Deretic, 1997; Dong and Wu, 2007). But, to date, no data are available on its implication in the neuronal traffic of receptors. When we identified Rab6 in our proteomic experiment, it appeared that the peptides digested from Rab6 identified by mass spectrometry were common to the two Rab6A isoforms (A and A′) but were different from Rab6B. GST pull-down experiments followed by Western blot analysis with Rab6 and tubulin antibodies further confirmed the presence of these proteins in the 5-HT$_{1A}$R interacting complex using the WT GST-CT1A as a bait but not with control GST alone or with the KdiR mutated GST-CT1A (Fig. 3*B*). In addition, Yip1A was also detected in the same complex with the GST-CT1A but not with the KdiR mutated GST-CT1A (Fig. 3*B*). These results suggested that the recruitment of Yip1A, Rab6, and tubulin within the receptor complex required the presence of Yif1B. Yip1A belongs to the same Yip family as Yif1B. Interaction between their ortholog Yip1p and Yif1p in yeast (Matern et al., 2000), or Yip1A and Yif1A in a human cell line (Jin et al., 2005) has been shown to play a role in vesicular docking to Golgi apparatus (Barrowman et al., 2003). No data are actually available on the interaction between Yif1B and Yip1A. Using GST-Rab6 (Fig. 3*C*) and the GST-Yip1A N-tail (Fig. 3*D*), we pulled down Yif1B, as expected from the existence of a direct interaction with Yif1B. Because we obtained the same results with both Rab6A and Rab6A′ (data not shown), we showed only the results obtained with the Rab6A isoform (labeled Rab6). Direct interaction between Yif1B and Rab6 or between Yif1B and Yip1A was further confirmed using SPR analysis, with purified GST-Rab6 and GST-Yip1A N-tail proteins loaded over the sensor chip grafted with the WT His-Yif1B N-tail. Yif1B interacted directly with Rab6 and the Yip1A N-tail with estimated K_D values of ~0.33 μM (Fig. 3*E*) and 1 μM (Fig. 3*F*), respectively. From these results, we hypothesized that Yif1B could cluster the 5-HT$_{1A}$R and other intracellular routing proteins like Yip1A and Rab6 in specialized transport vesicles carrying the receptor toward distal dendrites.

The 5-HT$_{1A}$R is colocalized in vesicles with its partner proteins Yif1B, Yip1A, and Rab6

Immunofluorescence experiments on transfected hippocampal neurons in culture were performed to visualize whether the 5-HT$_{1A}$R could be detected during its targeting in vesicles also labeled by the partner proteins Yif1B, Yip1A, and Rab6 identified above (Fig. 4). Because endogenous 5-HT$_{1A}$R could not be specifically detected in those cultures with all the antibodies we tested, we used Flag-tagged 5-HT$_{1A}$R (Flag-5-HT$_{1A}$R). We first confirmed the major plasma membrane localization of the 5-HT$_{1A}$R in somas and dendrites (Fig. 4*A1*) and found that the colocalization with endogenous Yif1B was more visible in den-

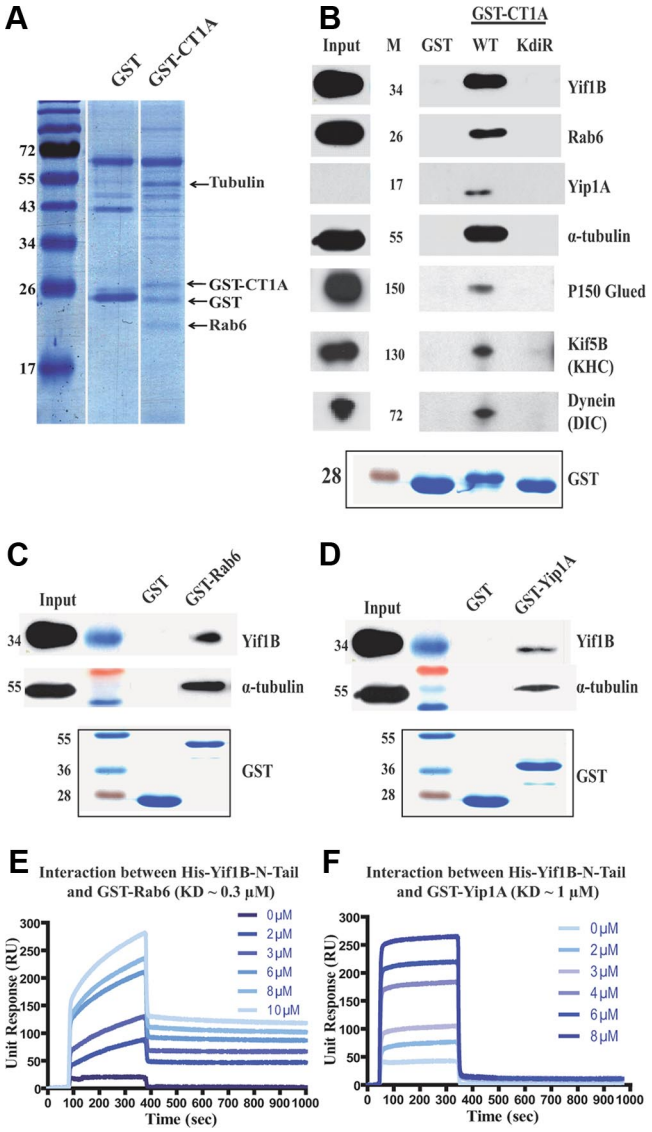

Figure 3. Rab6, Yip1A, tubulin, P150, Kif5B, and dynein interact with the 5-HT$_{1A}$R via Yif1B. ***A***, GST pull-down experiments with the WT GST-CT1A and GST alone as a control on rat brain extracts separated by a one-dimensional 12% SDS-PAGE stained by Colloidal Blue before identification by mass spectrometry. ***B–D***, GST pull-down experiments performed on rat brain lysates with purified WT (***B***) or KdiR GST-CT1A (***C***) purified GST-Rab6 or GST-Yip1A N-tail (***D***) and GST alone (negative control). GST pull-downs were analyzed by Western blot followed by ECL+ detection, and illustrations result from experiments loaded on the same gel. GST proteins were visualized using Coomassie Blue (bottom panels). Inputs represent a 2.5% load of the total lysates used in all conditions. Western blots (top panels) were revealed using anti-Yif1B (***B–D***), anti-Rab6 (***B***), anti-Yip1A (***B***), anti α-tubulin (***B–D***) antibodies, anti-P150 Glued (***B***), anti-Kif5B heavy chain (***B***), and anti-dynein intermediate chain (***B***). ***E***, ***F***, Kinetic studies of the interaction between GST-Rab6 (***E***) or the N-tail of GST-Yip1A (***F***) and WT His-Yif1B determined by surface plasmon resonance. The concentration range was 0–10 μM for GST-Rab6 (***E***) and 0–8 μM for the N-tail of GST-Yip1A (***F***) in six serial dilutions passed over His-Yif1B immobilized on a sensor chip ($n = 2$). Data are presented as real-time graphs of response unit (RU) against time and were analyzed using a 1:1 Langmuir binding model.

drites than in the soma (Fig. 4*A2*, arrows). On the other hand, Flag-5-HT$_{1A}$R and endogenous Rab6 and Yip1A were scarcely colocalized in the soma (Fig. 4*B*,*C*, arrows), and their endogenous expression in dendrites was too low to visualize an eventual colocalization. Yip1A exhibited a vesicular localization in the soma mainly around the Golgi apparatus identified by the expression of Rab6-eGFP. We found that Yip1A and Rab6 did occasionally colocalize in the same puncta (Fig. 4*E*). However, these puncta represented only a minor fraction of each population.

When we transfected the KdiR mutated Flag-5-HT$_{1A}$R that lost the capacity to interact with Yif1B, it remained sequestrated in large intracellular clusters in soma (Fig. 4*D1*), and we could not visualize specific colocalization in dendrites between the mutated KdiR receptor and Yif1B (Fig. 4*D2*) or with Rab6 and Yip1A (data not shown). The occasional colocalization observed in the soma seemed to result mainly from the intracellular aggregation of the mutant KdiR. In the soma, the strong aggregation of the KdiR Flag-5-HT$_{1A}$R apparently disorganized intracellular compartments and the distribution of endogenous markers.

Therefore, to study the colocalization of the three partners, we cotransfected neurons with a combination of two tagged proteins and stained for one endogenous partner (Fig. 5). In agreement with our previous results, Yif1B was mainly localized in somatic and dendritic intracellular vesicles (Fig. 5*A2*,*B2*,*C2*,*D2*). Yif1B was colocalized with the 5-HT$_{1A}$R in somatic vesicles that also expressed endogenous Rab6 (Fig. 5*A4*) or Yip1A (Fig. 5*B4*), this latter protein being associated with both somatic and dendritic vesicles (Fig. 5*B3*). Previous descriptions of Rab6 localization in neurons have shown a somatic Golgi localization and some colocalization with synaptophysin in immature neurons (Tixier-Vidal et al., 1993). In agreement with these data, we found Rab6 labeling on the Golgi in the soma (Fig. 4*A3*) and on vesicles in axons, compatible with its role in secretion (Grigoriev et al., 2007). Here, in addition, we visualized a clear labeling and trafficking in dendrites, suggesting that Rab6 also plays a role in the dendritic traffic (Fig. 5*C3*). We also observed some colocalization of the 5-HT$_{1A}$R (Fig. 5*C1*,*D1*) with Yif1B (Fig. 5*C2*,*D2*) and Rab6 (Fig. 5*C3*) or Yip1A (Fig. 5*D3*) in some dendritic vesicles, supporting our hypothesis that Yif1B could play the role of a scaffold protein in the complex targeting the 5-HT$_{1A}$R toward the dendrites. As a control, we investigated whether we could observe such colocalization with another neuronal GPCR expressed in neurons. We thus showed that some intracellular somatic vesicles containing the somatostatin sst2A-eGFP receptor partially colocalized with Rab6 protein, but were clearly not endowed with Yif1B or Yip1A (Fig. 6*A–C*).

Dynamic trafficking of the 5-HT$_{1A}$R and its partner proteins in living neurons

Because we wanted to go further in the study of the dynamics of dendritic targeting of the 5-HT$_{1A}$R with its partner proteins, we then focused on vesicles emanating from the soma and entering dendrites. We thus visualized the vesicular trafficking of the fluorescent-tagged 5-HT$_{1A}$R (Fig. 7*A1*), Yif1B (Fig. 7*A2*), Rab6 (Fig. 7*A3*), and Yip1A (Fig. 7*A4*) using time-lapse videomicroscopy in primary cultures of living hippocampal neurons. Whereas it was difficult to identify single vesicles expressing tagged 5-HT$_{1A}$R, Yif1B, Rab6, and Yip1A in fixed neurons, live confocal imaging demonstrated that these proteins were clustered within somatic intracellular mobile vesicles that oscillate in the soma. We also visualized the rapid traffic of these vesicles exhibiting a stop-and-go motion. Mean velocities were calculated after manual tracking, separately for the go periods that reached a mean velocity of 0.4–0.8 μm/s for 5–10 s, a motion usually followed by episodes with a lower speed, 0.1–0.2 μm/s (Fig. 7*B*). Vesicles that exited the soma toward the dendrites were also visualized for 5-HT$_{1A}$R, Yif1B, Rab6, and Yip1A, and were isolated in small movies (see Notes). In the dendrites, they all exhibited both anterograde and retrograde movements (Fig. 7*B*). The vesicles positive for Yip1A moved slightly more rapidly in the dendrites in comparison with Yif1B, Rab6, and the 5-HT$_{1A}$R, around 0.8 and 0.7 μm/s for anterograde (Fig. 7*B1*) and retrograde (Fig.

7*B2*) trajectories, respectively, suggesting that Yip1A could be included in the complex in the soma and might be separated in the dendrites. We could visualize vesicles positive for the 5-HT$_{1A}$R and Yif1B exiting the soma toward a dendrite (Fig. 7*C*). These vesicles moved at the same speed: ~0.4 μm/s (Fig. 7*B*) for both anterograde and retrograde movements. In conclusion, these movies demonstrated that the 5-HT$_{1A}$R and its partners exit the soma toward the dendritic tree in vesicles with equivalent speed supporting the hypothesis that they could be involved in the 5-HT$_{1A}$R targeting toward the distal dendrites and that they all exhibit anterograde and retrograde motion in dendrites.

The 5-HT$_{1A}$R undergoes vesicular bidirectional transport along dendritic microtubules

On one hand, α and β tubulins were identified as proteins interacting with the C-tail of the 5-HT$_{1A}$R by a proteomic approach (Fig. 3*A*), and, on the other hand, Western blot analysis showed that, unlike its WT form, the mutated KdiR form of the 5-HT$_{1A}$R, devoid of affinity for Yif1B (Fig. 2*B*), also lost the interaction with tubulin, suggesting that the presence of Yif1B is required for 5-HT$_{1A}$R interaction with the microtubules, as is the case with Rab6 and Yip1A (Fig. 3*B*). Furthermore, tubulin was pulled down with GST-Rab6 (Fig. 3*C*, middle) and the N-tail of GST-Yip1A (Fig. 3*D*, middle), indicating that tubulin interacts with these partners and is involved in the 5-HT$_{1A}$R traffic. We then verified the presence of the 5-HT$_{1A}$R and its partner proteins in vesicles along the dendritic microtubules (data not shown). Finally, to test microtubule dependency on this transport, neurons were treated with nocodazole at 10 μM for 1 h (Guillaud et al., 2003). Treatment of hippocampal cultures induced a disorganization of the dendritic distribution of 5-HT$_{1A}$R and also of all of its partners (data not shown), further supporting the idea that the microtubule network plays a key role in the dendritic trafficking of the 5-HT$_{1A}$R.

Yip1A, Rab6, and Kif5B play a crucial role in the distal dendritic targeting of the 5-HT$_{1A}$R

Because we visualized a vesicular trafficking in the dendrites together with a tight association with the microtubules, we searched for molecular motors that could explain the bidirectional trafficking of 5-HT$_{1A}$R-containing vesicles. Previous studies showed that Rab6 may interact ei-

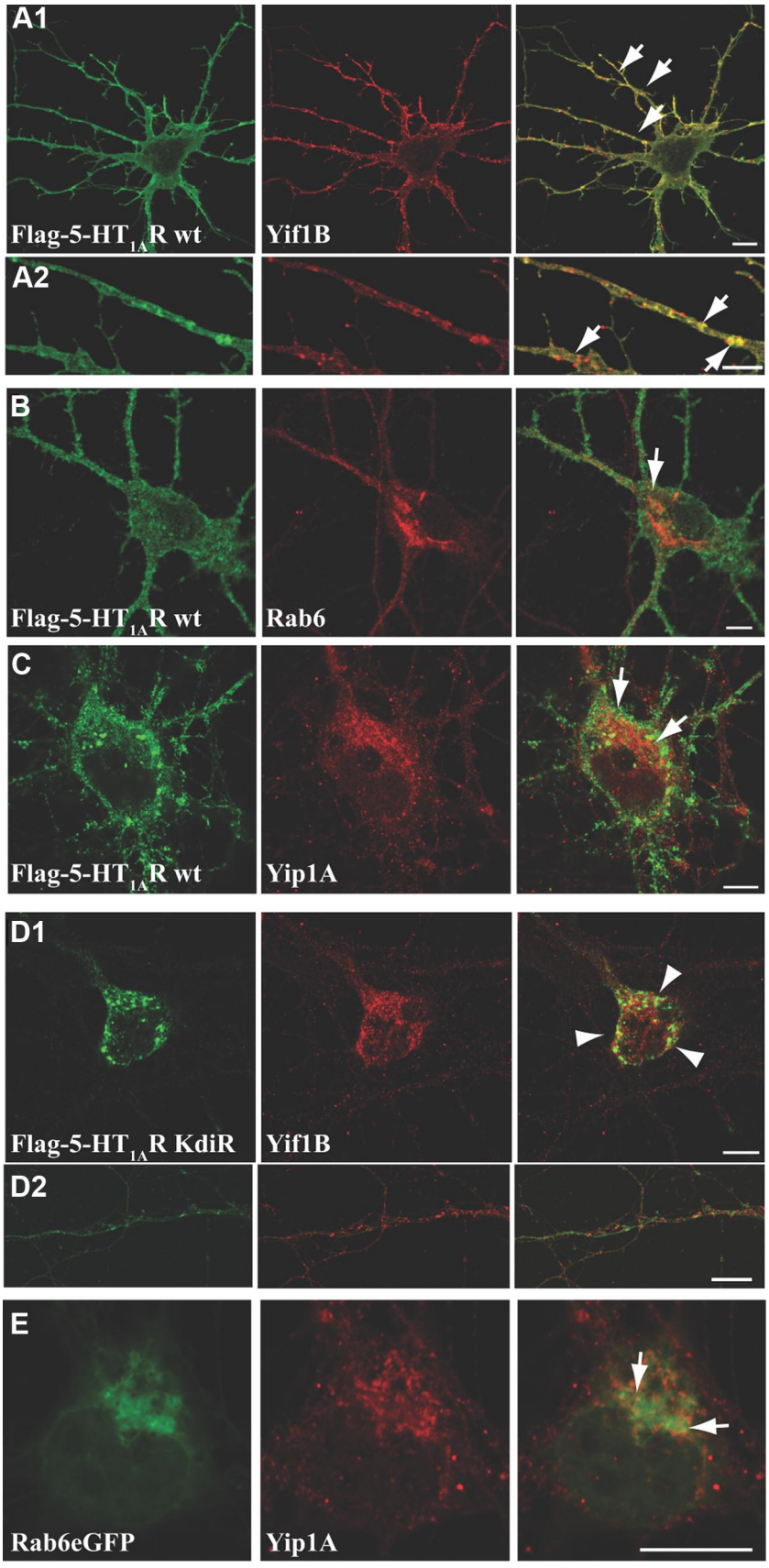

Figure 4. Colocalization between WT or mutated 5-HT$_{1A}$R and endogenous Yif1B, Yip1A, and Rab6 in neurons. ***A–D***, Hippocampal neurons were transfected at DIV7 with the Flag-5-HT$_{1A}$R wt (***A–C***) or the Flag-5-HT$_{1A}$R KdiR mutant (***D***) and labeled 48 h post-transfection for endogenous Yif1B (***A1***, ***A2***, ***D1***, ***D2***), Rab6 (***B***), or Yip1A (***C***) in red. ***E***, Colocalization of Rab6-eGFP and endogenous Yip1A. Some punctate colocalizations are shown by arrows in overlay; arrowheads show large intracellular clusters of the Flag-5-HT$_{1A}$R KdiR. Scale bars, 10 μm.

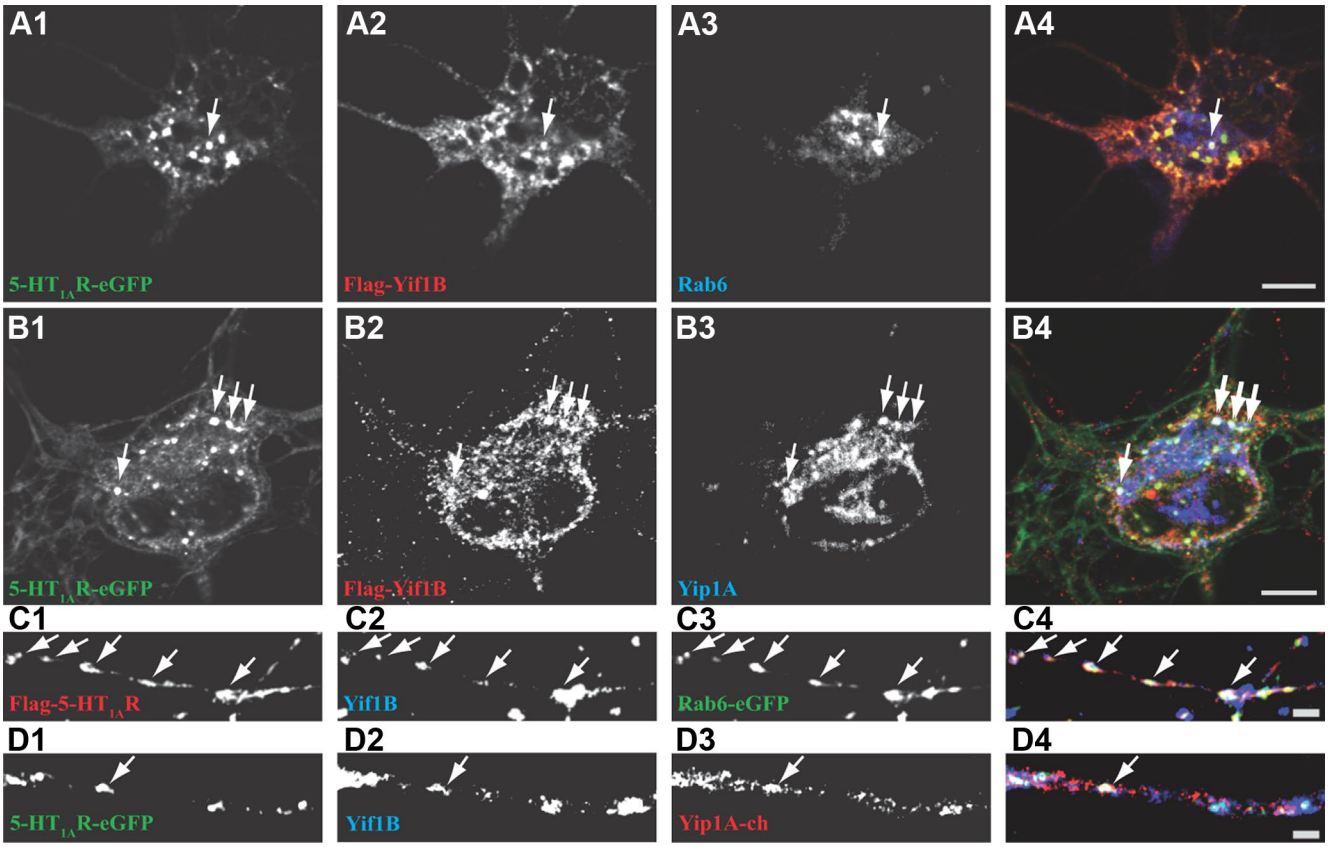

Figure 5. The 5-HT$_{1A}$R/Yif1B complex colocalizes with Rab6 and Yip1A in somatic and dendritic vesicles. ***A***, ***B***, ***D***, Hippocampal neurons were cotransfected at DIV 7 with the 5-HT$_{1A}$R-eGFP receptor (***A1***, ***B1***, ***D1***) and Flag-Yif1B (***A2***, ***B2***) and labeled 48 h post-transfection with the anti-Flag antibody in red (***A2***, ***B2***) and for endogenous Rab6 (***A3***) or Yip1A (***B3***) in blue. The Flag-5-HT$_{1A}$R was labeled with anti-Flag antibody in red (***C1***), Rab6-eGFP (***C3***) shown in green and endogenous Yif1B labeled with anti-Yif1B in blue (***C2***, ***D2***), or with Yip1A-Cherry in red (***D3***). Some punctate colocalizations are shown by arrows. ***A4–D4***, Overlay. Scale bars, 10 μm.

ther with a plus end-directed Kif5B (Grigoriev et al., 2007) or with a minus end-directed dynein (Wanschers et al., 2008). This led us to investigate their eventual interaction with the 5-HT$_{1A}$R.

Using GST pull-down experiments, in addition to Yif1B, Yip1A, Rab6, and tubulin we found two molecular motors in the complex interacting with the C-tail of the 5-HT$_{1A}$R: the kinesin Kif5B and the dynein (Fig. 3*B*). We also found the presence of p150Glued, a subunit of the dynactin complex that was shown to coordinate a bidirectional motion using opposite motors (Gross et al., 2002). All these proteins were not found when the GST pull-down experiment was performed with the mutated KdiR form of the 5-HT$_{1A}$R, devoid of affinity for Yif1B, suggesting that Yif1B was necessary for the interaction with these molecular motors (Fig. 3*B*).

We then studied the role of Yip1A, Rab6, and these molecular motors in the dendritic targeting of the 5-HT$_{1A}$R using RNA interference experiments on primary cultures of hippocampal neurons. In neurons transfected with 5-HT$_{1A}$R-eGFP alone (Fig. 8*A*) or with control siRNA (Fig. 8*E*), immunofluorescence of the receptor was visualized in distal dendrites. Depletion of endogenous Yip1A, Rab6, and Kif5B by siRNA was verified by Western blot experiments (Fig. 8*G1–G3*). After depletion of Yip1A (Fig. 8*B*), Rab6 (Fig. 8*C*), and Kif5B (Fig. 8*D*), the expression level of the 5-HT$_{1A}$R-eGFP was similar to control conditions (Fig. 8*F*), whereas the 5-HT$_{1A}$R-eGFP labeling was confined to the proximal portion of the dendrites. Quantification of the cumulated fluorescence intensity for 20 neurons in each condition along the longest dendrite provided evidence of the inhibitory effect of siRNA-mediated inhibition of Yip1A, Rab6, or KiF5B expression on the dendritic targeting of the 5-HT$_{1A}$R-eGFP (Fig. 8, right). Mean fluorescence along dendrites at 50–100 μm from the soma was significantly lower after RNA interference of Yip1A, Rab6, and Kif5B (Fig. 8*H*). This effect was not due to changes in dendritic morphology, since the labeling of α-tubulin was not modified by these siRNAs (Fig. 8, tubulin). We concluded that, in addition to Yif1B (Carrel et al., 2008), Yip1A, Rab6, and Kif5B also play a crucial role in the distal dendritic targeting of the 5-HT$_{1A}$R, thus defining a new complex trafficking pathway toward dendrites. As we showed previously that Yif1B plays a specific role for the 5-HT$_{1A}$R compared with the sst2A-eGFP receptor (Carrel et al., 2008), we also investigated the effect of depletion of Yip1A (Fig. 9*B*), Rab6 (Fig. 9*C*), and Kif5B (Fig. 9*D*) on sst2A-eGFP, and showed that neither Yip1A nor Kif5B depletion affected its dendritic localization whereas Rab6 depletion slightly diminished its traffic toward dendrites. The latter effect can be connected with the colocalization observed between sst2A-eGFP and Rab6 (Fig. 6*B*) and suggests that Rab6 could be crucial for the dendritic targeting of other neuronal receptors by using a Yif1B-independent scaffolding complex.

Discussion

Although Yif1B is a relatively ubiquitous protein, it clearly plays a specific targeting role in 5-HT$_{1A}$R trafficking toward distal dendrites in neurons. Here, we describe the molecular mechanisms involved in the interaction between Yif1B and the 5-HT$_{1A}$R. In a first step, we identified the motifs involved in their direct inter-

action and then searched for other proteins interacting with the 5-HT$_{1A}$R/Yif1B complex. Our data allow us to propose a new dendritic trafficking pathway in which Yif1B is the scaffold protein recruiting the 5-HT$_{1A}$R in a complex including Yip1A and Rab6, with Kif5B and dynein as molecular motors coordinating the bidirectional traffic of vesicles along dendritic microtubules. These data not only provide new insights into the cellular and molecular mechanisms underlying 5-HT$_{1A}$R trafficking, but also support the idea that the Yif1B-based dendritic transport described for the 5-HT$_{1A}$R could be shared with other neuronal receptors/channels.

A tribasic motif within the C-tail of the 5-HT$_{1A}$R is crucial for the interaction with Yif1B

In a previous study (Carrel et al., 2008), we have demonstrated that the interaction between Yif1B and the C-tail of the 5-HT$_{1A}$R is crucial for the dendritic targeting of the receptor. Here, using the surface plasmon resonance technology with purified proteins, we confirmed that this interaction is direct (Fig. 1*D*) and characterized by a high affinity (K_D = 37 nM). Moreover, we demonstrated that three aspartate residues located in the 30–50 aa region of the N-tail of Yif1B interact with a tribasic motif composed of one lysine in position 405 and a di-arginine motif in position 421–422 (corresponding to the KdiR mutant) within the C-tail of the 5-HT$_{1A}$R (Table 1). Interestingly, in addition to the presence of three positive charges, the position of the lysine seems crucial for the interaction since we showed that the K412diR mutant did not lose the interaction with Yif1B (Fig. 1; Table 1). Such a KdiR motif implicated in a protein–protein interaction has never been described previously.

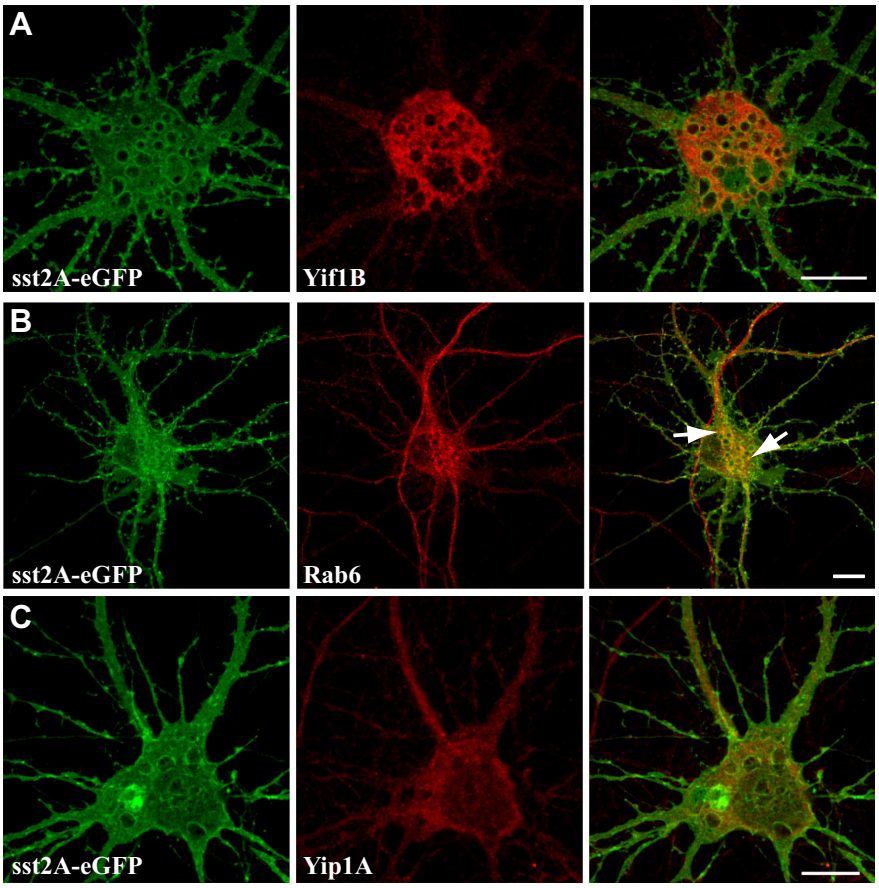

Figure 6. Colocalization between Yif1B, Yip1A, or Rab6 and the sst2A-eGFP receptor. ***A–C***, Hippocampal neurons were transfected at DIV7 with the sst2A-eGFP (***A–C***) and labeled 48 h post-transfection for the endogenous Yif1B (***A***) Rab6 (***B***), or Yip1A (***C***) in red. Some punctate colocalizations are shown by arrows in overlay with Rab6 (***B***). Scale bars, 10 μm.

The 5-HT$_{1A}$R is targeted to the dendrites by a novel vesicular scaffolding-dependent transport pathway

Our results allowed the description of a novel pathway that involves Yif1B as a scaffold protein clustering the 5-HT$_{1A}$R, Rab6, and Yip1A in the same vesicles trafficking toward the distal dendrites in hippocampal neurons (Fig. 8). Four lines of evidence support this hypothesis: first, GST pull-down results showed that the 5-HT$_{1A}$R interacts with Rab6 and Yip1A through the implication of Yif1B, since this interaction was lost with the KdiR mutant, devoid of affinity for Yif1B (Figs. 3*B*, 4). Second, surface plasmon resonance experiments demonstrated that Yif1B interacts directly with the 5-HT$_{1A}$R (Fig. 1*D*), Rab6 (Fig. 3*E*), and Yip1A (Fig. 3*F*). Third, vesicles containing the 5-HT$_{1A}$R/Yif1B complex and endogenous Rab6 or Yip1A could be detected in somas and dendrites of fixed neurons (Figs. 4, 5). Finally, we found that 5-HT$_{1A}$R trafficking was also dependent on the expression of Rab6 and Yip1A, since the depletion of these two proteins by RNA interference induced the disruption of the dendritic targeting of the receptor (Fig. 8) in a similar way as inhibition of Yif1B expression (Carrel et al., 2008). Whereas the role of Yip1A as a targeting protein is herein described for the first time, Rab6 was already reported to be involved in the trafficking of several GPCRs. It has been implicated in the traffic of rhodopsin in photoreceptor cells (Deretic, 1997), in the targeting to the plasma membrane of the β2 adrenergic and the angiotensin 1 receptors in HeLa cells (Dong and Wu, 2007), and also in exocytosis of neurotransmitters in axons (Grigoriev et al., 2007), but never as a dendritic targeting protein. This new pathway involves different proteins compared with other routing mechanisms such as those described for NMDA or AMPA receptors, using CASK, SAP97, or GRIP1 (Wyszynski et al., 1999; Dong and Wu, 2007; Jeyifous et al., 2009) which rely on motifs interacting with PDZ domain-containing proteins. Indeed, these motifs do not exist in the 5-HT$_{1A}$R. In contrast, we identified a new tribasic interaction motif. It cannot be excluded that this Yif1B-dependent dendritic transport in which Rab6 and Yip1A participate, could also be used by other dendritic receptors through the implication of multiple scaffolding complexes.

Yif1B is the scaffold protein between Rab6 and Yip1A

In cell lines, the subcellular localization of Yif1B has been restricted neither to the Golgi nor to the endoplasmic reticulum, but more probably to the intermediate compartment (Carrel et al., 2008). In primary cultures of hippocampal neurons, our results showed that Yif1B colocalizes scarcely with Rab6 and partially with Yip1A, in the somas of neurons (Fig. 5). Furthermore, Rab6 was found mainly in the somatic Golgi, in agreement with the results describing the subcellular localization of this protein

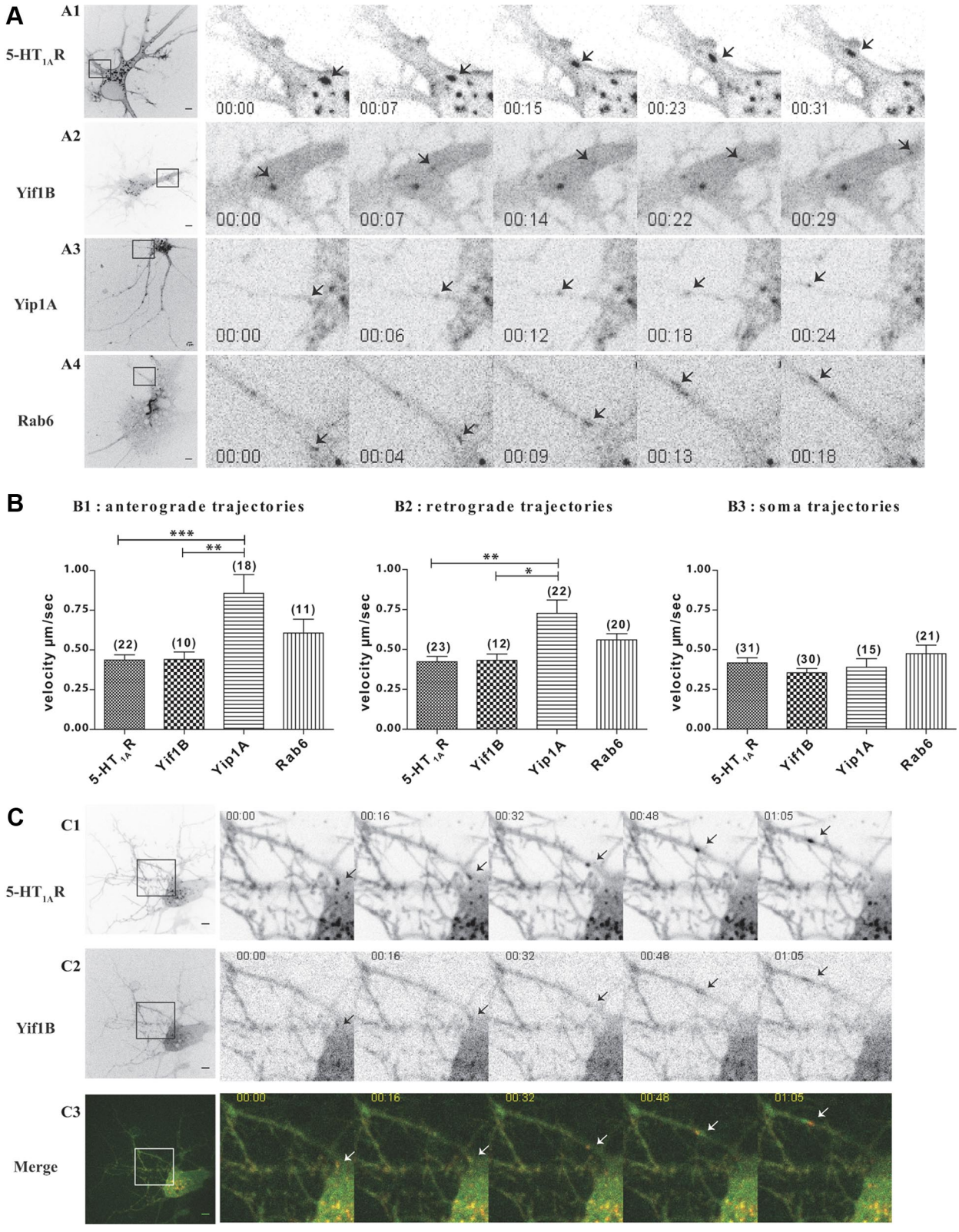

Figure 7. The 5-HT$_{1A}$R and its partners traffic in mobile vesicles exiting from the soma toward dendrites. ***A***, Inverted monochrome images from time-lapse imaging of hippocampal neurons expressing the 5-HT$_{1A}$R-cherry (***A1***), Yif1B-eGFP (***A2***), Rab6-eGFP (***A3***), and Yip1A-cherry (***A4***). Left panels show the whole field, with a boxed area corresponding to the zoom on proximal dendrites. Arrows follow the labeled vesicles during their anterograde dendritic transport. Scale bars, 5 μm. ***B***, Mean velocities of moving vesicles. Trajectories of moving vesicles were tracked with the MTrackJ Plugin of ImageJ software. Trajectories were classified as anterograde (***B1***) or retrograde (***B2***) according to their direction in dendrites or as somatic (***B3***) if the traffic occurred only in the soma. Bar graphs show mean + SEM, calculated and plotted using GraphPad 4 Software. Numbers of trajectories are indicated in parentheses above bar graphs. ***$p < 0.0001$, **$p < 0.001$, *$p < 0.05$ (one-way ANOVA with Bonferroni's *post hoc* test). ***C***, Time-lapse imaging 2 d after the transfection of hippocampal neurons with the 5-HT$_{1A}$R-cherry and Yif1B-eGFP. Inverted monochrome images of the 5-HT$_{1A}$R (***C1***) and Yif1B-eGFP (***C2***). Double-labeled migrating puncta are visualized in the overlay (***C3***). Left panels show the whole field, with a boxed area corresponding to the zoom on proximal dendrites. Arrows point at the particles during their anterograde dendritic transport. Scale bars, 5 μm.

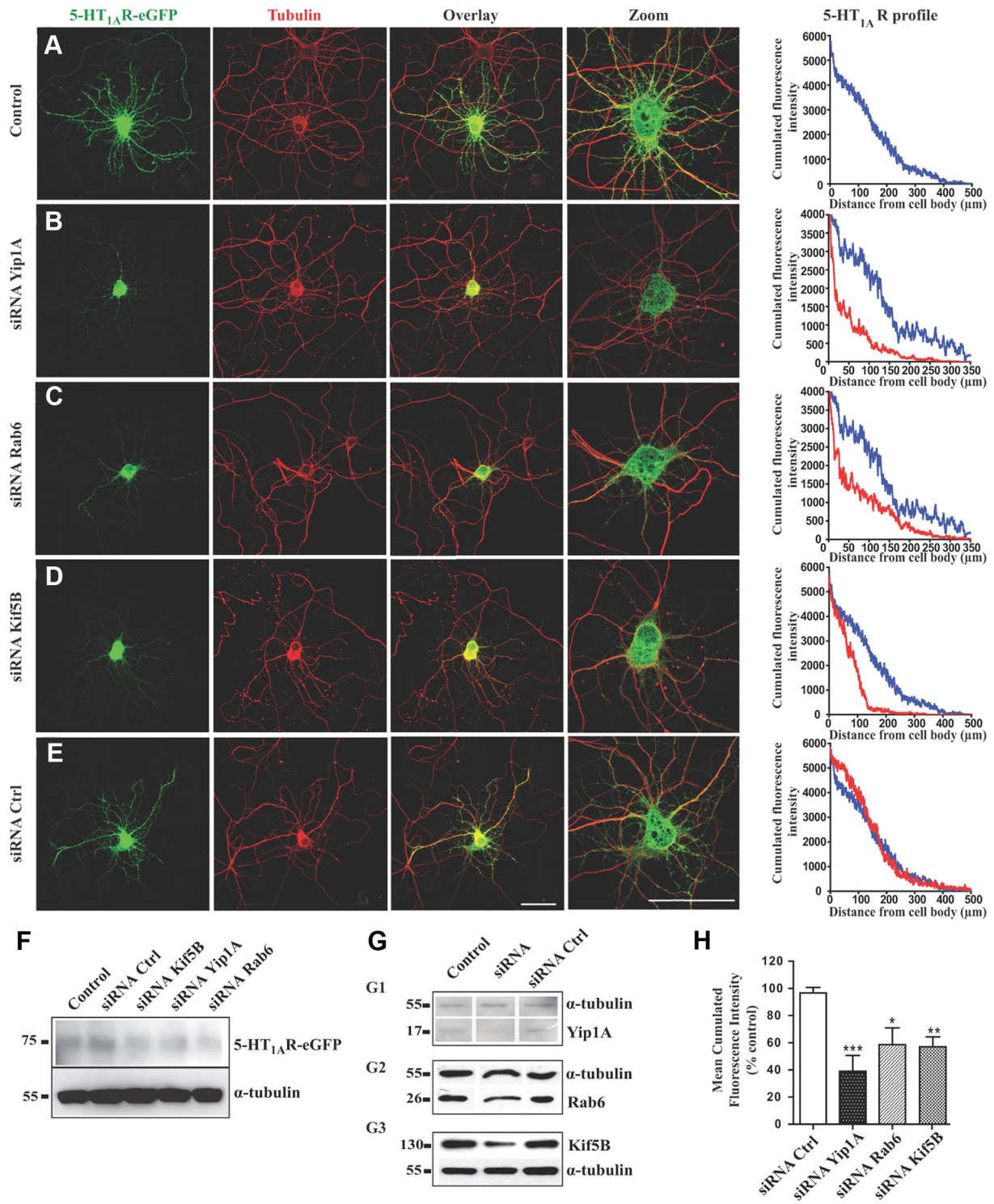

Figure 8. Yip1A, Rab6, or Kif5B depletions disturb 5-HT$_{1A}$R targeting toward distal dendrites. ***A–E***, Immunofluorescence of neurons transfected with the 5-HT$_{1A}$R-eGFP alone (***A***) or cotransfected with the 5-HT$_{1A}$R-eGFP plus siRNAs against endogenous Yip1A (***B***), endogenous Rab6 (***C***), endogenous Kif5B (***D***), or control siRNA (***E***). Immunolabeling was performed with anti-GFP antibody to enhance the GFP signal (green, left) or anti-α-tubulin antibody (red, middle). Overlay and zoom on the soma are shown on the right. On the right panels, the graphs represents the cumulated fluorescence intensities of the 5-HT$_{1A}$R (cumulated fluorescence intensity, arbitrary unit) along the longest dendrite of monitored neurons (μm), in control conditions (blue) compared with experimental conditions (red) with siRNA against Yip1A, Rab6 or Kif5B. Scale bars, 50 μm. ***F***, Expression level of the 5-HT$_{1A}$R-eGFP was similar in siRNA-transfected neurons in comparison with control conditions after visualization on Western blot of protein extracts 48 h after transfection of neurons at DIV7. ***G***, Downregulation of the Yip1A, Rab6, and Kif5B proteins by siRNAs in primary cultures of rat hippocampal neurons 48 h after transfection of neurons at DIV7. Yip1A (***G1***), Rab6 (***G2***), and Kif5B (***G3***) were detected by Western blots of protein extracts; α-tubulin was immunolabeled in the same membrane to normalize the amount of extract. All neurons were cotransfected with 5-HT$_{1A}$R-eGFP alone (Control) or with 5-HT$_{1A}$R-eGFP plus siRNA directed against endogenous Yip1A, Rab6, or Kif5B, or control siRNA. ***H***, Normalized average 5-HT$_{1A}$R fluorescence in dendrites along 50–100 μm from soma. Mean fluorescence at 50 μm was calculated for 20 neurons for each condition and then normalized to the mean value of the control condition [siRNA(control), siRNA(Yip1A), siRNA(Rab6), and siRNA(Kif5B)]. The fluorescence of 5-HT$_{1A}$R is significantly lower in dendrites after siRNA-induced downregulation of Kif5B, Rab6, or Yip1A. $N = 20–30$ neurons per condition. Bar graphs show mean + SEM. *$p < 0.05$, **$p < 0.01$ ***$p <$ 0.001 (one-way ANOVA with Dunnett's multiple comparison *post hoc* test).

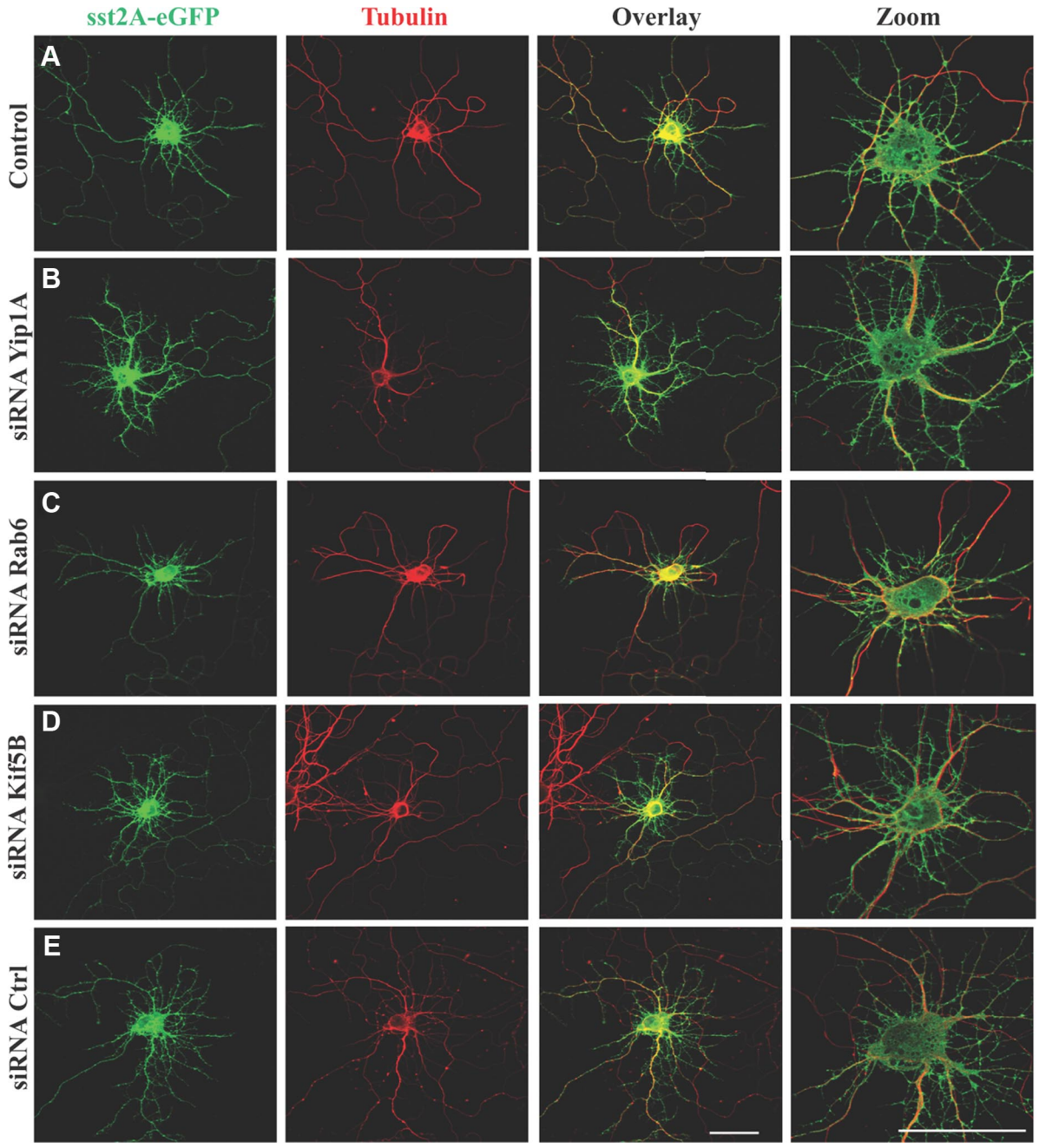

Figure 9. Effect of Yip1A, Rab6, and Kif5B depletions on sst2A-eGFP targeting toward distal dendrites. ***A–E***, Immunofluorescence of neurons transfected with the sst2A-eGFP alone (***A***) or cotransfected with the sst2A-eGFP plus siRNAs against endogenous Yip1A (***B***), endogenous Rab6 (***C***), endogenous Kif5B (***D***), or control siRNA (***E***). Immunofluorescence was performed with an anti-GFP antibody to enhance the GFP signal (green, left) or an anti-α-tubulin antibody (red, middle). Right, Overlay and zoom on the soma. Scale bars, 50 μm.

(Tixier-Vidal et al., 1993), but also in mobile dendritic vesicles in hippocampal neurons. In addition, we demonstrated that Yif1B interacted with Yip1A or Rab6 with good affinities (Fig. 3). An interaction between Yip1A and Yif1A, the homologue of Yif1B, has already been reported in HeLa cells, with the implication of Yip1A in the Golgi localization of Yif1A (Jin et al., 2005). Accordingly, we could suggest that Yip1A might play the same function concerning Yif1B. Finally, we also showed that Rab6 colocalizes partially with Yip1A in vesicles around the somatic Golgi in neurons (Fig. 4*E*). Altogether our results suggest that Yif1B could be the protein mediating the indirect interaction between Rab6 and Yip1A whose expression is crucial for the Golgi localization of Rab6 (Kano et al., 2009).

Vesicles containing the Yif1B scaffolding complex are transported along the microtubule network by two opposite molecular motors coordinating the bidirectional motion

Because tubulin has been characterized as one of the proteins bound to the 5-HT$_{1A}$R/Yif1B multimolecular complex, it was likely that we were dealing here with a scaffold structure anchoring the 5-HT$_{1A}$R to the microtubule cytoskeleton (Fig. 10). In line with this hypothesis, several studies showed that Rab6 is transported along microtubules through an interaction with various molecular motors (Matanis et al., 2002; Short et al., 2002; Miserey-Lenkei et al., 2010), including the kinesin-like protein Rabkinesin6 (Echard et al., 1998).

Therefore, our hypothesis was that 5-HT$_{1A}$R trafficking along the microtubules could result from an interaction between Rab6

and molecular motors. Indeed, in addition to the crucial role of Rab6 in the dendritic transport of the 5-HT$_{1A}$R (Fig. 8), we found that tubulin interacts with Rab6 in brain (Fig. 3*C*). Whereas Rab6 containing vesicles have been shown to traffic between the Golgi and the endoplasmic reticulum (Martinez et al., 1997) or between the Golgi and the plasma membrane (Valente et al., 2010) in cell lines, much less is known regarding the role of Rab6 in neurons. To date, it has been implicated only in neuritogenesis (Schlager et al., 2010) and in the regulation of the transport and targeting of exocytotic carriers toward axon terminals (Grigoriev et al., 2007). Here, our data support the idea that Rab6 also participates in the Yif1B-dependent transport pathway that is crucial for the 5-HT$_{1A}$R trafficking toward the dendrites along microtubules. In the Yif1B scaffolding complex, Rab6 could play the role of an intermediate adaptor for the control of molecular motors, ensuring the traffic of the receptor along microtubule tracks. Interestingly, we found two molecular motors in the complex interacting with the C-tail of the 5-HT$_{1A}$R: the dynein that steers to the minus-end of microtubules, and Kif5B that steers to the plus-end of microtubules (Fig. 3). Microtubules exhibit a mixed polarity in proximal dendrites, whereas in distal dendrites they exhibit a minus-to-plus end polarity. As Kif5B moves toward the plus end of microtubules, it could participate in the anterograde transport of the receptor. In that case, retrograde transport of the receptor in distal dendrites could rely on the dynein motor. But as the dynein/dynactin complex interacts with the 5-HT$_{1A}$R (Fig. 3), we cannot exclude that dynein could play a role in the initial sorting in proximal dendrite microtubules as it was proposed for the initial sorting of dendritic cargo (Kapitein et al., 2010). Accordingly, the dynein/dynactin complex could interact with Rab6 in the first part of the trafficking of the receptor, as was described for the secretory vesicle transport (Schlager et al., 2010). This would imply a switch of molecular motors during the dendritic transport, which could rely on the presence of P150 in the complex (Fig. 3*B*).

In conclusion, we describe here for the first time the Yif1B scaffolding complex that clusters the 5-HT$_{1A}$ receptor with Yip1A and Rab6 in vesicles transported along the microtubule network using specific molecular motors for the receptor addressing to distal dendrites. This novel Yif1B-dependent trafficking pathway could be shared by other GPCRs or other neuronal receptors/channels.

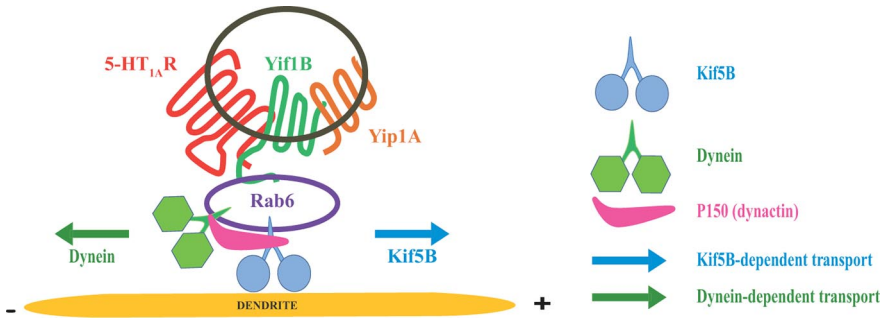

Figure 10. Schematic representation of the Yif1B scaffolding complex involved in 5-HT$_{1A}$R trafficking toward dendrites. According to the model built from the data reported herein, the Yif1B-dependent transport would involve Yif1B as the scaffold protein assembling the 5-HT$_{1A}$R, Yip1A, and Rab6 in the same vesicles trafficking along the dendritic microtubules, using two opposite molecular motors, the conventional kinesin Kif5B and the dynein for their bidirectional movements. The dynactin subunit P150 would enable switching between molecular motors for the bidirectional transport observed in the dendrites. Rab6 might play the role of an intermediate protein for the interaction of these molecular motors with the Yif1B scaffolding complex.

Notes

Supplemental material for this article is available at http://minilien.fr/a0nahr. Time-lapse video microscopy is shown using DIV9 hippocampal neurons in culture, expressing fluorescent-tagged 5-HT$_{1A}$R, Yif1B, Yip1A, or Rab6. The movies were taken with a spinning-disk confocal microscope, at an image acquisition rate of 1 image/s. Images represent a maximal projection of a *z*-stack acquired at each time point, with a time exposure of 50–200 ms, depending on the protein. Representation is in inverted monochrome. This material has not been peer reviewed.

References

Albert PR, Zhou QY, Van Tol HH, Bunzow JR, Civelli O (1990) Cloning, functional expression, and mRNA tissue distribution of the rat 5-hydroxytryptamine1A receptor gene. J Biol Chem 265:5825–5832.

Barrowman J, Wang W, Zhang Y, Ferro-Novick S (2003) The Yip1p.Yif1p complex is required for the fusion competence of endoplasmic reticulum-derived vesicles. J Biol Chem 278:19878–19884. CrossRef Medline

Björk K, Sjögren B, Svenningsson P (2010) Regulation of serotonin receptor function in the nervous system by lipid rafts and adaptor proteins. Exp Cell Res 316:1351–1356. CrossRef Medline

Bockaert J, Perroy J, Bécamel C, Marin P, Fagni L (2010) GPCR interacting proteins (GIPs) in the nervous system: roles in physiology and pathologies. Annu Rev Pharmacol Toxicol 50:89–109. CrossRef Medline

Bortolozzi A, Castañé A, Semakova J, Santana N, Alvarado G, Cortés R, Ferrés-Coy A, Fernández G, Carmona MC, Toth M, Perales JC, Montefeltro A, Artigas F (2012) Selective siRNA-mediated suppression of 5-HT(1A) autoreceptors evokes strong anti-depressant-like effects. Mol Psychiatry 17:612–623. CrossRef Medline

Brewer CB, Roth MG (1991) A single amino acid change in the cytoplasmic domain alters the polarized delivery of influenza virus hemagglutinin. J Cell Biol 114:413–421.

Carrel D, Hamon M, Darmon M (2006) Role of the C-terminal di-leucine motif of 5-HT1A and 5-HT1B serotonin receptors in plasma membrane targeting. J Cell Sci 119:4276–4284. CrossRef Medline

Carrel D, Masson J, Al Awabdh S, Capra CB, Lenkei Z, Hamon M, Emerit MB, Darmon M (2008) Targeting of the 5-HT1A serotonin receptor to neuronal dendrites is mediated by Yif1B. J Neurosci 28:8063–8073. CrossRef Medline

Del Nery E, Miserey-Lenkei S, Falguières T, Nizak C, Johannes L, Perez F, Goud B (2006) Rab6A and Rab6A' GTPases play non-overlapping roles in membrane trafficking. Traffic 7:394–407. CrossRef Medline

Deretic D (1997) Rab proteins and post-Golgi trafficking of rhodopsin in photoreceptor cells. Electrophoresis 18:2537–2541. CrossRef Medline

Dong C, Wu G (2007) Regulation of anterograde transport of adrenergic and angiotensin II receptors by Rab2 and Rab6 GTPases. Cell Signal 19:2388–2399. CrossRef Medline

Doucet E, Latrémolière A, Darmon M, Hamon M, Emerit MB (2007) Immunolabelling of the 5-HT 3B receptor subunit in the central and peripheral nervous systems in rodents. Eur J Neurosci 26:355–366. CrossRef Medline

Duvernay MT, Dong C, Zhang X, Zhou F, Nichols CD, Wu G (2009) Anterograde trafficking of G protein-coupled receptors: function of the C-terminal F(X)6LL motif in export from the endoplasmic reticulum. Mol Pharmacol 75:751–761. CrossRef Medline

Echard A, Jollivet F, Martinez O, Lacapère JJ, Rousselet A, Janoueix-Lerosey I, Goud B (1998) Interaction of a Golgi-associated kinesin-like protein with Rab6. Science 279:580–585. CrossRef Medline

Escoffier P, Paris L, Bodaghi B, Danis M, Mazier D, Marinach-Patrice C (2012) Pooling aqueous humor samples: bias in 2D-LC-MS/MS strategy? J Proteome Res 9:789–797.

Goslin K, Asmussen H, Banker G (1998) Rat hippocampal neurons in low-density culture. In: Culturing nerve cells, Ed 2 (Banker G, Goslin K, eds), pp 339–370. Cambridge, MA: MIT.

Grigoriev I, Splinter D, Keijzer N, Wulf PS, Demmers J, Ohtsuka T, Modesti M, Maly IV, Grosveld F, Hoogenraad CC, Akhmanova A (2007) Rab6

regulates transport and targeting of exocytotic carriers. Dev Cell 13:305–314. CrossRef Medline

Gross SP, Welte MA, Block SM, Wieschaus EF (2002) Coordination of opposite-polarity microtubule motors. J Cell Biol 156:715–724. CrossRef Medline

Guillaud L, Setou M, Hirokawa N (2003) KIF17 dynamics and regulation of NR2B trafficking in hippocampal neurons. J Neurosci 23:131–140. Medline

Jeyifous O, Waites CL, Specht CG, Fujisawa S, Schubert M, Lin EI, Marshall J, Aoki C, de Silva T, Montgomery JM, Garner CC, Green WN (2009) SAP97 and CASK mediate sorting of NMDA receptors through a previously unknown secretory pathway. Nat Neurosci 12:1011–1019. CrossRef Medline

Jin C, Zhang Y, Zhu H, Ahmed K, Fu C, Yao X (2005) Human Yip1A specifies the localization of Yif1 to the Golgi apparatus. Biochem Biophys Res Commun 334:16–22. CrossRef Medline

Jolimay N, Franck L, Langlois X, Hamon M, Darmon M (2000) Dominant role of the cytosolic C-terminal domain of the rat 5-HT$_{1B}$ receptor in axonal-apical targeting. J Neurosci 20:9111–9118. Medline

Kano F, Yamauchi S, Yoshida Y, Watanabe-Takahashi M, Nishikawa K, Nakamura N, Murata M (2009) Yip1A regulates the COPI-independent retrograde transport from the Golgi complex to the ER. J Cell Sci 122:2218–2227. CrossRef Medline

Kapitein LC, Schlager MA, Kuijpers M, Wulf PS, van Spronsen M, MacKintosh FC, Hoogenraad CC (2010) Mixed microtubules steer dynein-driven cargo transport into dendrites. Curr Biol 20:290–299. CrossRef Medline

Laemmli UK (1970) Cleavage of structural proteins during the assembly of the head of bacteriophage T4. Nature 227:680–685.CrossRef Medline

Lelouvier B, Tamagno G, Kaindl AM, Roland A, Lelievre V, Le Verche V, Loudes C, Gressens P, Faivre-Baumann A, Lenkei Z, Dournaud P (2008) Dynamics of somatostatin type 2A receptor cargoes in living hippocampal neurons. J Neurosci 28:4336–4349. CrossRef Medline

Le Poul E, Laaris N, Doucet E, Laporte AM, Hamon M, Lanfumey L (1995) Early desensitization of somato-dendritic 5-HT1A autoreceptors in rats treated with fluoxetine or paroxetine. Naunyn Schmiedebergs Arch Pharmacol 352:141–148. Medline

Martinez O, Antony C, Pehau-Arnaudet G, Berger EG, Salamero J, Goud B (1997) GTP-bound forms of rab6 induce the redistribution of Golgi proteins into the endoplasmic reticulum. Proc Natl Acad Sci U S A 94:1828–1833. CrossRef Medline

Matanis T, Akhmanova A, Wulf P, Del Nery E, Weide T, Stepanova T, Galjart N, Grosveld F, Goud B, De Zeeuw CI, Barnekow A, Hoogenraad CC (2002) Bicaudal-D regulates COPI-independent Golgi-ER transport by recruiting the dynein-dynactin motor complex. Nat Cell Biol 4:986–992. CrossRef Medline

Matern H, Yang X, Andrulis E, Sternglanz R, Trepte HH, Gallwitz D (2000) A novel Golgi membrane protein is part of a GTPase-binding protein complex involved in vesicle targeting. EMBO J 19:4485–4492. CrossRef Medline

Miserey-Lenkei S, Chalancon G, Bardin S, Formstecher E, Goud B, Echard A (2010) Rab and actomyosin-dependent fission of transport vesicles at the Golgi complex. Nat Cell Biol 12:645–654. CrossRef Medline

Oksche A, Dehe M, Schülein R, Wiesner B, Rosenthal W (1998) Folding and cell surface expression of the vasopressin V2 receptor: requirement of the intracellular C-terminus. FEBS Lett 424:57–62. CrossRef Medline

Perrot A, Pionneau C, Nadaud S, Davi F, Leblond V, Jacob F, Merle-Béral H, Herbrecht R, Béné MC, Gribben JG, Bahram S, Vallat L (2011) A unique proteomic profile on surface IgM ligation in unmutated chronic lymphocytic leukemia. Blood 118:e1–e15. CrossRef Medline

Prybylowski K, Chang K, Sans N, Kan L, Vicini S, Wenthold RJ (2005) The synaptic localization of NR2B-containing NMDA receptors is controlled by interactions with PDZ proteins and AP-2. Neuron 47:845–857. CrossRef Medline

Riad M, Garcia S, Watkins KC, Jodoin N, Doucet E, Langlois X, el Mestikawy S, Hamon M, Descarries L (2000) Somatodendritic localization of 5-HT1A and preterminal axonal localization of 5-HT1B serotonin receptors in adult rat brain. J Comp Neurol 417:181–194. Medline

Schlager MA, Kapitein LC, Grigoriev I, Burzynski GM, Wulf PS, Keijzer N, de Graaff E, Fukuda M, Shepherd IT, Akhmanova A, Hoogenraad CC (2010) Pericentrosomal targeting of Rab6 secretory vesicles by Bicaudal-D-related protein 1 (BICDR-1) regulates neuritogenesis. EMBO J 29:1637–1651. CrossRef Medline

Shevchenko A, Tomas H, Havlis J, Olsen JV, Mann M (2006) In-gel digestion for mass spectrometric characterization of proteins and proteomes. Nat Protoc 1:2856–2860. CrossRef Medline

Short B, Preisinger C, Schaletzky J, Kopajtich R, Barr FA (2002) The Rab6 GTPase regulates recruitment of the dynactin complex to Golgi membranes. Curr Biol 12:1792–1795. CrossRef Medline

Stockmeier CA, Shapiro LA, Dilley GE, Kolli TN, Friedman L, Rajkowska G (1998) Increase in serotonin-1A autoreceptors in the midbrain of suicide victims with major depression-postmortem evidence for decreased serotonin activity. J Neurosci 18:7394–7401. Medline

Szewczyk B, Albert PR, Rogaeva A, Fitzgibbon H, May WL, Rajkowska G, Miguel-Hidalgo JJ, Stockmeier CA, Woolverton WL, Kyle PB, Wang Z, Austin MC (2010) Decreased expression of Freud-1/CC2D1A, a transcriptional repressor of the 5-HT(1A) receptor, in the prefrontal cortex of subjects with major depression. Int J Neuropsychopharmacol 13:1089–1101. CrossRef Medline

Tixier-Vidal A, Barret A, Picart R, Mayau V, Vogt D, Wiedenmann B, Goud B (1993) The small GTP-binding protein, Rab6p, is associated with both Golgi and post-Golgi synaptophysin-containing membranes during synaptogenesis of hypothalamic neurons in culture. J Cell Sci 105:935–947. Medline

Valente C, Polishchuk R, De Matteis MA (2010) Rab6 and myosin II at the cutting edge of membrane fission. Nat Cell Biol 12:635–638. CrossRef Medline

Wanschers B, van de Vorstenbosch R, Wijers M, Wieringa B, King SM, Fransen J (2008) Rab6 family proteins interact with the dynein light chain protein DYNLRB1. Cell Motil Cytoskeleton 65:183–196. CrossRef Medline

White J, Johannes L, Mallard F, Girod A, Grill S, Reinsch S, Keller P, Tzschaschel B, Echard A, Goud B, Stelzer EH (1999) Rab6 coordinates a novel Golgi to ER retrograde transport pathway in live cells. J Cell Biol 147:743–760. CrossRef Medline

Wyszynski M, Valtschanoff JG, Naisbitt S, Dunah AW, Kim E, Standaert DG, Weinberg R, Sheng M (1999) Association of AMPA receptors with a subset of glutamate receptor-interacting protein *in vivo*. J Neurosci 19:6528–6537. Medline